11 Muon-catalyzed fusion (μCF)

[K. Nagamine]

11.1 Introduction

Muon-catalyzed fusion (μCF) is a nuclear fusion reaction mediated by a short-lived, negatively charged, accelerator-produced elementary particle called muon (μ^-) which is similar to a heavy electron. Once μCF becomes feasible to be applied as an energy source, it yields several important advantages compared to other methods of fusion energy, namely no need of high temperature, running under complete control and high spatial fusion density. Unfortunately, the development of μCF towards a sizable contribution to fusion energy has been delayed because of limited access to muon-producing accelerators. However, some progress has been made during the last years by the experimental and theoretical effort of the μCF-related scientists. The goal of this chapter is to describe the present status of understanding of the μCF phenomena and the future perspective of μCF contributing to fusion energy.

The presentation is structured as follows. After an introduction to the basic properties of muons (Sect. 11.2), muon production at particle accelerators is described (Sect. 11.3), as well as the behaviour of μ^- after injection inside matter and the formation of muonic hydrogen atoms (Sect. 11.4). Then the basic concept of μCF (Sect. 11.5) and the present μCF experiments (Sect. 11.6) are discussed. An account of μCF phenomena in deuterium-tritium (D-T) mixtures is given, considering the fusion reaction in a small molecule formed by participation of the μ^- (Sect. 11.7), followed by a description of μ^- transfer from deuterium to tritium taking place right after the formation of the muonic atom (Sect. 11.8). Then the formation process of the (dtμ) molecule where a rapid fusion reaction takes place is discussed (Sect. 11.9). Additional μCF phenomena limiting the energy production are described, namely muon-to-alpha sticking right after the fusion reaction in the (dtμ) molecule as well as its ionization (μ^- regeneration) during the slowing-down of the stuck $(\mu\alpha)^+$ ion (Sect. 11.10). This is followed by an account of the inherent problem of the He impurity effect (Sect. 11.11). Finally, future perspectives of μCF as an energy source are considered, with special emphasis on the realization of a μCF power generator at the kW level (Sect. 11.12).

Numerical data used as functional relationships in the figures are compiled in Sect. 11.15.

11.2 Basic properties of muons

The properties of muons can be summarized as follows. Muons (μ^- and their anti-particles, μ^+) are unstable, charged elementary particles with a spin of 1/2. Their mass lies between the proton and the electron mass (1/9 m_p and 207 m_e), and their mean lifetime is approximately 2.2 μs. Muons were first discovered in cosmic rays in 1937 [37And]. The vertical flux of cosmic-ray muons at sea level is 1 $cm^{-2}min^{-1}$. Nowadays, muons are produced in large numbers by using particle accelerators. Some data relevant to muon science are summarized in Table 11.1.

The uniqueness of the muon lifetime and mass can be understood by comparing them with the values of other particles. The muon has the second longest lifetime among all unstable particles after the neutron, and the second smallest mass among all particles after the electron.

Muons are produced in pion decays according to

$$\pi^+ \rightarrow \mu^+ + \nu_\mu \,, \tag{11.1}$$

$$\pi^- \rightarrow \mu^- + \bar{\nu}_\mu \,. \tag{11.2}$$

Since the spin of the pion is zero and the muon neutrino has a definite helicity h such that $h = +1$ for $\bar{\nu}_\mu$ and $h = -1$ for ν_μ, the muon is 100 % polarized in the pion center-of-mass system.

The muon decays into an electron and two neutrinos as follows:

$$\mu^+ \rightarrow e^+ + \nu_e + \bar{\nu}_\mu , \tag{11.3}$$

$$\mu^- \rightarrow e^- + \bar{\nu}_e + \nu_\mu . \tag{11.4}$$

Again, as a result of parity violation, the decay electrons are distributed asymmetrically with respect to the muon polarization.

Table 11.1. Fundamental properties of muons. The charge is given in units of the elementary charge e. The magnetic moment is given as a multiple of the proton's magnetic moment μ_p. Uncertainties are written in parentheses.

	μ^+	μ^-
Charge [e]	+1	−1
Mass	206.768277(24) m_e [a])	105.659(1) MeV/c^2 [b])
Spin	1/2	1/2
Magnetic moment	3.18334513(39) μ_p [a])	
Gyromagnetic ratio $g/2$	1.0011659203(15) [c])	
Free-decay lifetime [10^{-6} s]	2.19695(6) [d])	2.1948(10) [f])
	2.197078(73) [e])	
Decay modes	$e^+ + \nu_e + \bar{\nu}_\mu$ (≈ 100 %)	
	$e^+ + \gamma$ ($< 1.7 \times 10^{-10}$)	
	$e^+ + e^- + e^+$ ($< 1.9 \times 10^{-9}$)	
	$e^+ + \gamma + \gamma$ ($< 1.25 \times 10^{-8}$)	

[a]) [99Liu], [b]) [86Bel], [c]) [01Bro], [d]) [84Gio], [e]) [84Bar], [f]) in flight [72Wil].

11.3 Accelerator-produced muons

Muons can most easily be obtained through the decay of pions produced in nuclear interactions between accelerated particles and nuclear targets. Today high-intensity proton accelerators are the most popular source of accelerated particles. In Table 11.2 a list of medium-energy proton accelerators currently in use for muon-physics research is presented. Most activities are based on accelerators of the so-called meson factories such as PSI (Switzerland) and TRIUMF (Canada) which have beams with an intensity of some 100 μA to some mA. From the viewpoint of time structure there are two types of accelerators, with either continuous or pulsed beams. At PSI and TRIUMF, the proton beam is continuous in a macroscopic sense and has a microscopic structure (intensity modulation) with a characteristic frequency of 51 MHz at PSI and 23 MHz at TRIUMF, respectively. This frequency is simply the radio frequency of the cyclotron producing the primary beam.

At KEK, the 500 MeV booster synchrotron for the 12 GeV main ring provides a single-bunch proton beam with 50 ns width and 20 Hz repetition frequency. Its pulse structure is quite unique: the pulse width is much shorter than the muon lifetime τ_μ, while the pulse separation is much longer than τ_μ. This feature provides sharply pulsed muons [81Nag]. A more advanced synchrotron generating 200 μA of 800 MeV protons with a pulse time-structure of a double 70 ns (340 ns separation) and 50 Hz repetition rate was originally built for the neutron spallation-source at the ISIS facility of the Rutherford Appleton Laboratory (RAL) and is now used by a European group for the production of intense, pulsed surface μ^+ [88Eat] and by the RIKEN group for the production of pulsed decay μ^+/μ^- and surface μ^+ [96Nag1, 01Mat].

At the beginning of the 21st century, there is some demand for the realization of further high-intensity proton accelerators including: (a) an intense neutron spallation-source at the level of 1 MW (e.g. 1 GeV × 1 mA) to 10 MW (e.g. 3 GeV × 3.3 mA) for applications as neutron-scattering experiments,

radioactive-waste disposal and accelerator-driven subcritical reactors; (b) an intense muon source at the MW level to be used for a neutrino factory, for a $\mu^+\mu^-$ collider, for rare muon-decay searches or for a μCF-based 14 MeV neutron source.

The energy of accelerated protons in proton-proton reactions should be greater than twice the pion mass (282 MeV/c^2). By using a nuclear target, this condition becomes somewhat relaxed due to the kinetic energy of the nucleons inside the nucleus. Typical examples of pion-production cross sections in proton-nucleus reactions are summarized in Fig. 11.1. Qualitative understanding of the pion-production mechanism can be obtained from the Δ-resonance model [57Lin] by considering the formation of Δ-resonance states in nucleon-nucleon scattering being the dominant contribution to the production, with relevant corrections due to relativistic kinematics and phase-space limitations.

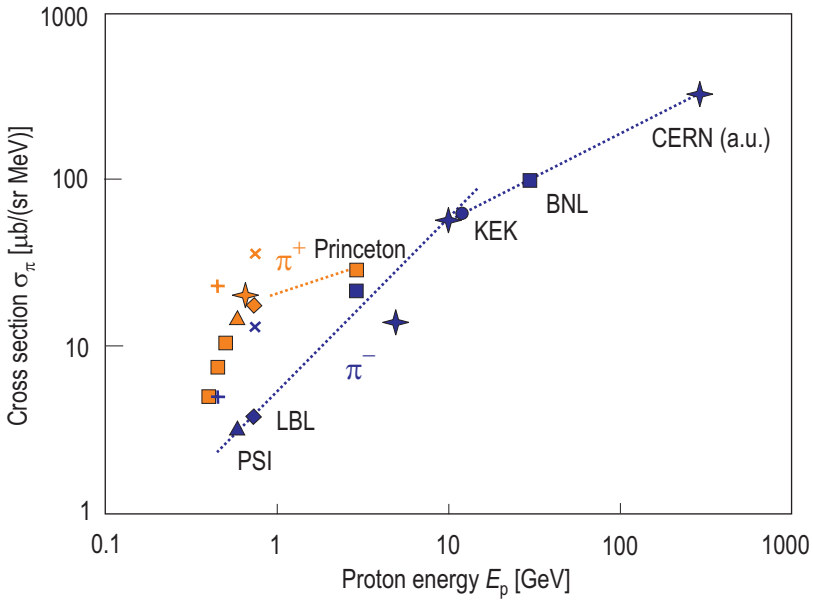

Fig. 11.1. Production cross sections of 50 MeV pions at 90 degrees in proton-nucleus (carbon) reactions [00Ish].

For the purpose of efficient pion production, the primary proton energy is typically chosen around 500…800 MeV. In this range, the most intense pion flux is produced at forward angles. The pion beam is contaminated by a large number of electrons originating from π^0 decays. In order to obtain a muon beam of high purity, this electron contamination must be eliminated in the beam channel. It is worth noting that at energies of 500…800 MeV the π^+ yield is four times higher than the π^- yield.

There are three types of muon production according to the spatial position (with respect to the target) where $\pi \rightarrow \mu$ decays take place. These are "decay μ", "cloud μ" and "surface μ".

Pions are produced by nuclear processes when a target is hit by high-energy protons. The momentum spectrum and the angular distribution of the pions produced depend on the primary beam energy as well as on the target used (Figs. 11.2 and 11.3).

The decay length of pions of momentum p_π is

$$L_\pi[\text{cm}] = c\,\beta\gamma\tau_\pi = 5.593 \times p_\pi\,[\text{MeV}/c]\,, \tag{11.5}$$

where β is υ/c, $\tau_\pi = 2.6 \times 10^{-8}$ s is the mean lifetime of the pion at rest and $m_\pi = 140$ MeV/c^2 is the pion rest mass. To produce muons by in-flight pion decays, one needs pions of moderate momenta in the range 100…200 MeV/c, where the pion decay length is 5.6…11.2 m.

In the $\pi \rightarrow \mu$ decay, the muon momentum in the pion rest frame is 29.8 MeV/c and its direction is isotropic. In the laboratory frame, where the pion moves with momentum p_π, the muon momentum has a flat distribution between the two limits

$$P_\mu^{\mathrm{Fw}} = (\beta_\pi + \beta_\mu^*)\, p_\pi / [\beta_\pi (1 + \beta_\mu^*)] , \tag{11.6}$$

$$P_\mu^{\mathrm{Bw}} = (\beta_\pi - \beta_\mu^*)\, p_\pi / [\beta_\pi (1 + \beta_\mu^*)] , \tag{11.7}$$

where $\beta_\mu^* = 0.2714$ is the muon velocity according to a momentum of 29.80 MeV/c in the pion rest frame. These limits correspond to forward and backward decays, respectively, in the pion rest frame. Since muons with momenta close to either of these limits move along the initial pion direction, they are easy to transport. Furthermore, they have definite polarizations of +1 and −1, respectively. Backward muons are of particular interest because their momentum (about half of p_π) is far from the initial beam momentum and so they can be cleanly separated from other particles such as pions or electrons by magnetic means. In addition, muons of lower momentum have a higher stopping density.

The muon-momentum distribution for a given pion momentum and the corresponding decay angle in the laboratory frame are schematically shown in Figs. 11.2. and 11.3, respectively.

Table 11.2. Typical examples of proton accelerators used for muon production.

	Energy [GeV]	Particles per pulse	Repetition rate [Hz]	Current [μA]
KEK PS Booster (Japan)	0.5	0.2×10^{13}	20	6
LAMPF PSR (USA)	0.8			100
Rutherford ISIS (UK)	0.8	2.5×10^{13}	50	200
SNS (USA) [a])	1.25			4000
J-PARC 3GeV (Japan) [a])[b])	3	8.3×10^{13}	25	333
CERN PS (Switzerland)	26	0.2×10^{13}	0.50	1.60
KEK PS (Japan)	12	0.4×10^{13}	0.25	0.16
BNL AGS (USA)	30	6×10^{13}	0.30	3.00
Serpukov (Russia)	70	1.7×10^{13}	0.10	0.27
J-PARC 50GeV (Japan) [a])[b])	50	30×10^{13}	0.30	15.00

[a]) Under construction, [b]) JAERI-KEK joint project of high-intensity proton accelerator.

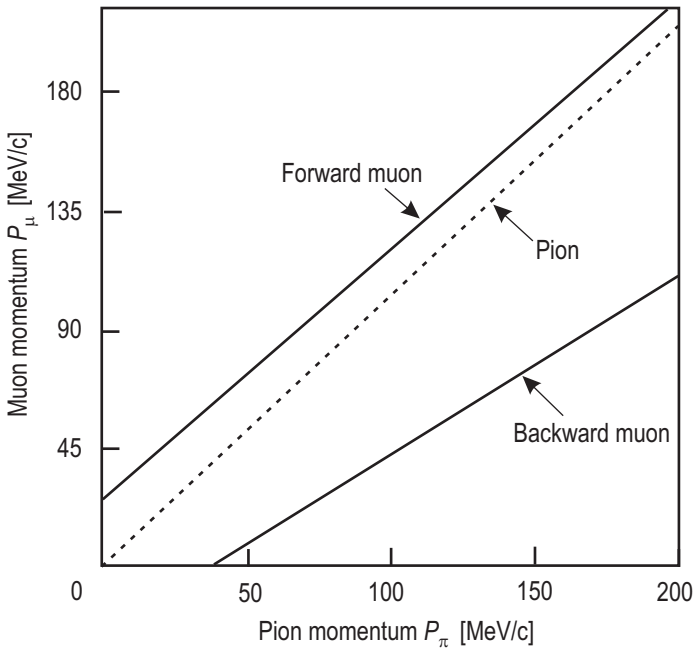

Fig. 11.2. Properties of muons produced in pion decays in flight: momentum distribution.

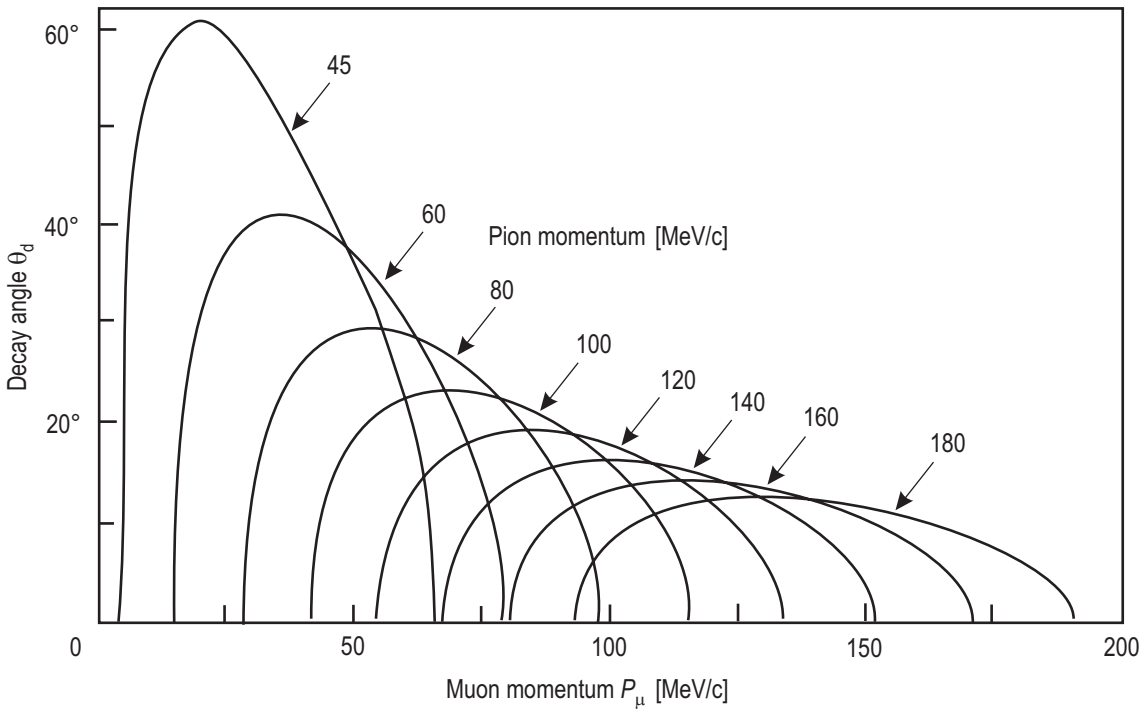

Fig. 11.3. Properties of muons produced in pion decays in flight: decay-cone aperture angle.

11.4 Muons inside matter and muonic atoms

Let us consider a μ^+ or μ^- with an energy in the range from several MeV to several ten MeV which after production by some conventional intermediate-energy accelerator is introduced into condensed matter. For μ^-, the time-dependent changes corresponding to the various energy-loss processes as well as the changes of polarization are displayed in Fig. 11.4. At energies higher than a few keV, where there is not much difference between μ^+ and μ^-, the main mechanism of energy loss is ionization which is described by the Bethe-Bloch formula.

A μ^- reaching the end of the ionization regime will be strongly attracted by the electric fields of the nuclei. The μ^- replaces an electron from the innermost atomic shell (K shell) to form a muonic atom in an excited state with the critical quantum number $n_c = (m_\mu/m_e)^{1/2} = 14$. Actual populations of each state of (n, ℓ_n) are widely distributed.

In the various cascade transitions occurring in the muonic atom (μ^-Z) after its formation by atomic capture of the muon in isolated atoms and molecules, there is a competition between radiative processes emitting X-ray photons, $(\mu^-Z)_n \rightarrow (\mu^-Z)_{n'} + \gamma$, and (external) Auger processes which emit low-energy electrons from the atom's inner shell, $(\mu^-Z)_n + Z' \rightarrow (\mu^-Z)_{n'} + Z'^{+} + e^-$. Generally speaking, radiative transitions dominate over Auger transitions in cases where the transition-energy gap is large [58Wes]. In addition, in some molecules, molecular dissociation, $(\mu^-Z)_n + (Z')^2 \rightarrow (\mu^-Z)_{n'} + Z' + Z'$, becomes the dominant source of cascade transitions [80Bor]. Also, among different orbital quantum numbers, Stark-mixing must be taken into account, $(\mu^-Z)_{n,\ell} + Z' \rightarrow (\mu^-Z)_{n',\ell'} + Z'$ $(n = n')$.

Some additional processes of the new cascade transition are now known to be significant, particularly in case of muonic hydrogen atoms (μ^-p, μ^-d and μ^-t) which appear in muon-catalyzed fusion. There is Coulomb de-excitation to accelerate and elastic scattering to decelerate the muonic atom. The Coulomb de-excitation is $(\mu^-p, \mu^-d, \mu^-t)_i + (p, d, t) \rightarrow (\mu^-p, \mu^-d, \mu^-t)_f + (p, d, t)'$ which becomes dominant over Auger transitions for $n > 10$ [78Bra]. There the muonic hydrogen has an energy gain of $\Delta E_{if}\,[m_p/(m_{\mu^-p} + m_p)]$ in case of $(\mu^-p)_i + p \rightarrow (\mu^-p)_f + p'$. On the other hand, during the elastic scattering process of $(\mu^-p, \mu^-d, \mu^-t)_i + (p, d, t) \rightarrow (\mu^-p, \mu^-d, \mu^-t)_f + (p, d, t)'$, owing to a transport cross section $\sigma_n^t = \pi\,(n^2-1)/m^*T$ for a state n, kinetic energy T and reduced mass m^*, the muonic hydrogen experiences an energy loss $\Delta T/T = \overline{(1-\cos\theta)}(2m_{\mu^-p} + m_H)/(m_{\mu^-p} + m_H)^2\,\sigma_n^t$ in the case of $(\mu^-p) + p$ elastic scattering at an angle θ.

As presented in the latest proceedings of the μCF conference [02Ish], the cascade kinetics related to the thermalization of muonic hydrogen atoms is one of the hot topics in theoretical studies. The involvement of the cascade kinetics in all the μCF processes described below is subject to be cleared, e.g. μ^- transfer or molecular formation before or after thermalization.

The ground state of a muonic atom, in which the μ^- passes most of its lifetime following the atomic cascade transitions, is characterized by the following properties: binding energy, size, lifetime and magnetic moment.

When the μ^- forms a muonic atom around a light nucleus with atomic number Z, the radius $R_\mu(1s)$ and the binding energy $E_\mu(1s)$ of the ground state can be described within the point-nucleus approximation as follows:

$$R_\mu(1s) \approx 270/Z \times 10^{-13}\ \text{cm}\,, \tag{11.8}$$

$$E_\mu(1s) \approx 13.6 \times 207 \times Z^2\ \text{eV}. \tag{11.9}$$

This remains a good approximation until the radius of the 1s orbital of the muonic atom becomes similar to that of the nucleus.

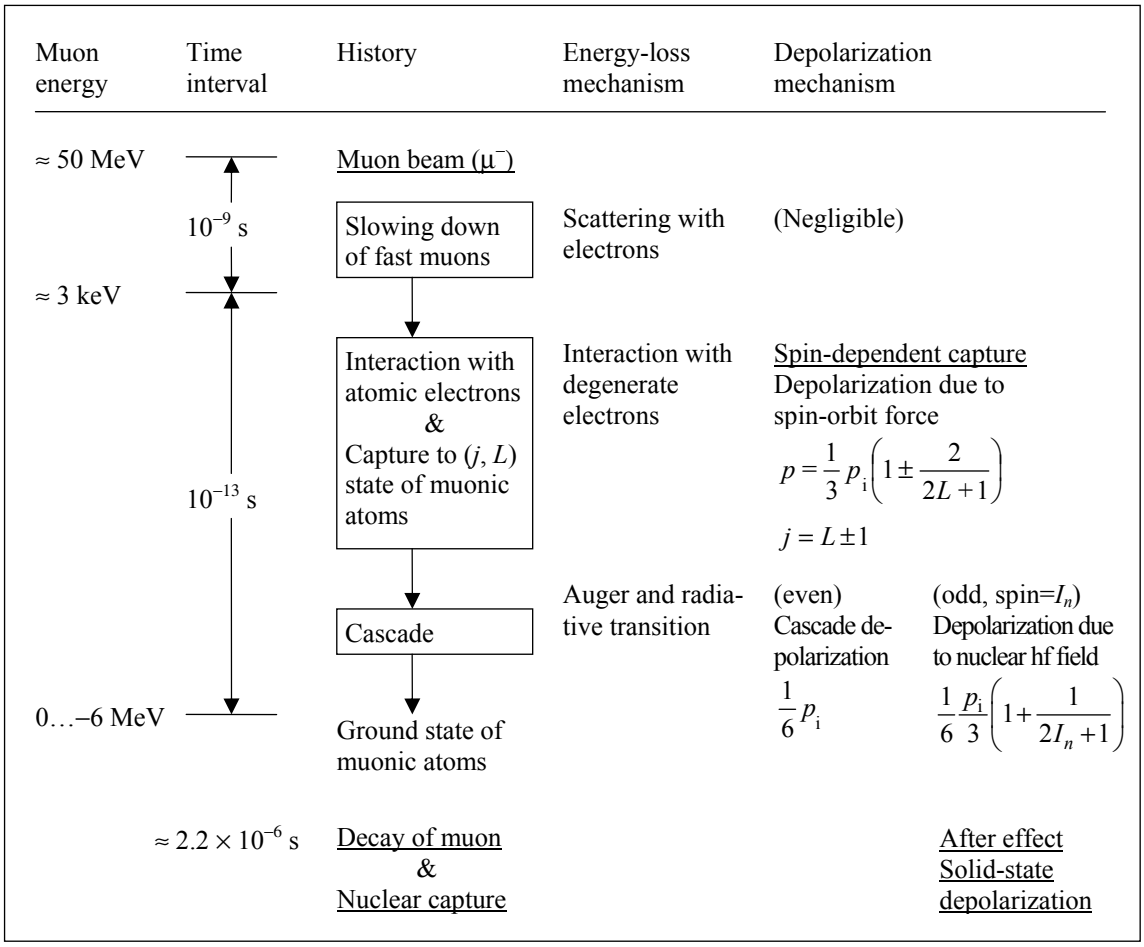

Fig. 11.4 History of a 50 MeV beam of negative muons introduced in condensed matter, including energy-loss and depolarization mechanisms.

The energy levels of muonic atoms differ significantly from the predictions of the classical point-nucleus approximation as a result of two factors: (1) the finite-sized nature of the nuclear charge distribution, and (2) vacuum polarization [77Hue]. Actually, the values of $E_\mu(nl)$ have long been used as a good measure of the nuclear charge distribution [74Eng].

The lifetime of the ground state is determined by the free muon decay rate, $\Lambda_0 = 1/\tau_\mu$, and the nuclear capture rate, Λ_c, which depends upon the Z number of the nucleus, $\tau_N^{-1} = \Lambda_o + \Lambda_c$. For higher Z nuclei, the capture rate becomes larger. The elementary nuclear capture process is $\mu^- + p \rightarrow n + \nu_\mu$. Since the capture rate is proportional to the spatial muon density at the nucleus, $[1/R_\mu(1s)]^3$ (proportional to Z^3), as well as to the proton number Z of the nucleus, Λ_c is proportional to Z^4 overall (the Z^4 law). Thus, the nuclear capture rate is given by the expression

$$\Lambda_c = \Lambda_1 Z^4, \tag{11.10}$$

where Λ_1 is the capture rate in the case of hydrogen. For heavier nuclei, however, the capture rate begins to differ significantly from the Z^4 law, and Λ_c has a saturation value around 0.1 μs^{-1} at $Z \approx 100$. For higher-Z elements, significant corrections to the Z^4 law are to be considered.

Basic properties of muonic hydrogen atoms (μp, μd and μt) which are essential for the understanding of muon-catalyzed fusion are summarized in Table 11.3.

Table 11.3. Basic properties of muonic hydrogen atoms.

	μp	μd	μt
1s binding energy E_{1s} [eV]	2528	2663	2711
1s hyperfine splitting ΔE_{hfs} [eV]	0.183 [c])	0.0482 [d])	0.2381 [d])
Nuclear capture rate λ_c [s^{-1}]	≈ 500 [a])	≈ 400 [a])	≈ 10 [b])

[a]) Experimental data summarized by Zavattini [75Zav].
[b]) Theoretical estimate [75Phi].
[c]) Values cited in the review [90Pon].
[d]) Theoretical estimate [01Bak].

11.5 Basic concept of muon catalysis of nuclear fusion

Of the two types of muons, only the μ^- is involved in μCF processes. As depicted in Fig. 11.5, nuclear fusion reactions take place when two nuclei such as d and t approach one another to within the range of the nuclear interaction, r_n (≈ a few times 10^{-13} cm). However, owing to the Coulomb repulsion between the positively charged nuclei which increases with decreasing distance, the realization of nuclear fusion is not at all easy. In the concept of thermal nuclear fusion, the required energy is given by thermal energy (kT) satisfying the condition $kT \geq e^2/r_n$. By assuming $r_n \approx 10^{-12}$ cm, the right-hand side of the inequality becomes 7×10^4 eV. In the μCF concept, the fusion reaction is mediated by a small neutral atom formed out of a μ^- and a hydrogen isotope and by the subsequent formation of a small muonic molecule. In this case, the relevant energy is the appropriate overall formation energy.

In addition to a possible future application as an energy source, the fascinating features in μCF research concern a variety of physical phenomena related to the interplay between nuclear and electromagnetic interactions. These features are strikingly exemplified by the case of deuterium-tritium (D-T) mixtures with a density ϕ comparably high as the liquid-hydrogen density, ϕ_0 (0.425×10^{23} nuclei/cm^3). In the following, the present understanding of μCF as well as future prospects for μCF research are summarized, with particular emphasis on D-T μCF. An overview of typical fusion reactions is given in Table 11.4.

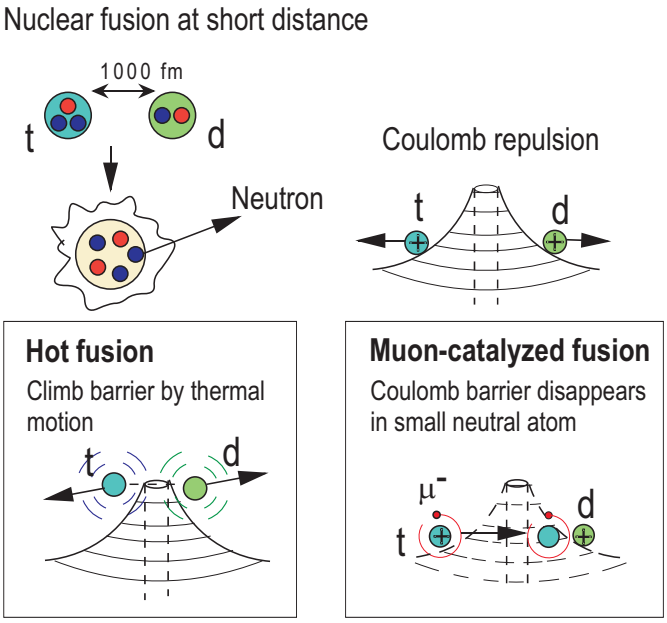

Fig. 11.5. Conceptual view of the role of a negative muon used to remove the repulsive potential between d and t in order to catalyze nuclear fusion, with reference to thermal nuclear fusion.

Table 11.4. Typical fusion reactions. The energy released is listed in brackets.

p + d	→	^{3}He + γ	(5.5 MeV)	d + t	→	4He + n	(17.6 MeV)
p + t	→	^{4}He + γ	(19.8 MeV)	t + t	→	^{4}He + 2n	(11.3 MeV)
d + d	→	^{3}He + n	(3.3 MeV)	d + ^{3}He	→	^{4}He + p	(18.4 MeV)
	→	t + p	(4 MeV)				
	→	^{4}He + γ	(24 MeV)				

The most basic μCF phenomena comprise the following two processes: (1) the formation of a small muonic molecule and a subsequent intramolecular fusion reaction, and (2) the mediation of a chain of fusion reactions by a single μ^-. These two processes are depicted in Figs. 11.6 and 11.7 for the case of D-T μCF. In the past, to highlight the muon's catalytic role, the chain reaction was sometimes presented in cyclic form as shown in Fig. 11.7. The basic process is summarized below. Details of the present level of understanding of each subprocess involved are given in the subsequent sections. After high-energy μ^- injection and stopping of the μ^- in a D-T mixture, either a (dμ) or a (tμ) atom is formed, with a probability more or less proportional to the relative concentrations C_d and C_t of deuterium and tritium, respectively ($C_d + C_t = 1$). Due to the difference between (dμ) and (tμ) in the binding energies of their atomic states (either excited or ground state), a μ^- initially in the atomic state (dμ) undergoes a transfer reaction to t yielding (tμ) during a collision with the surrounding t in either D-T or T_2 molecules. This reaction, written (dμ) + t → (tμ) + d, occurs at a rate λ_{dt}. The (tμ) thus formed, either before or after thermalization, reacts with D_2, DT, or T_2 to form a muonic molecule at a rate $\lambda_{dt\mu}$. Important in this step is the formation of a specific state of the (dtμ) molecule through a resonant mechanism. Once the (dtμ) molecule has been formed in this specific molecular state, a rapid cascade transition process of the μ^- inside the (dtμ) molecule takes place, followed by a fusion reaction occurring in a low-lying molecular state of the (dtμ) in which the distance between d and t is sufficiently small to allow for fusion. In the aftermath of this process, a 14.1 MeV neutron and a 3.7 MeV α-particle are emitted.

After the fusion reaction inside the (dtμ) molecule, most of the μ^- are liberated to participate in a further μCF cycle. A small fraction of the μ^-, however, is captured by the recoiling positively charged α particles. The probability of forming an $(\alpha\mu)^+$ ion is called the initial sticking probability ω_s^0. Once the $(\alpha\mu)^+$ is formed, since the μ^- has an initial kinetic energy of 90 keV compared to the 10 keV binding energy of the ground state of (αμ), the μ^- can be liberated again by stripping it from the $(\alpha\mu)^+$ ion. This process is called regeneration, with a corresponding fraction R. Thus, μ^- in the form of either a non-stuck μ^- or one regenerated from the $(\alpha\mu)^+$ can participate in a further μCF cycle, while the fraction of $(\alpha\mu)^+$ which thermalizes is left out from the μCF cycle, leading to an effective sticking parameter $\omega_s = (1-R)\,\omega_s^0$. Some additional details of the dtμ-μCF cycle are also shown in Fig. 11.7. In the (dμ) to t transfer process, there is a possibility that the μ^- is transferred from excited states of (dμ). Since t, d and μ^- have non-zero spin, there should be a hyperfine (spin-dependent) effect on the formation process of the muonic molecule. Moreover, the existence of a He impurity is inevitable because of t-decay and the μCF process itself, so that μ^- loss through capture by ^{3}He or ^{4}He must be taken into account.

Several different physical interactions are involved in the main processes of μCF. The fusion reaction taking place within the small muon molecule is the most significant part of the process where the nuclear interaction dominates, though there is some nuclear-interaction effect upon muon sticking and related processes, too. The remaining steps of the cycle hinge mainly on electromagnetic interactions, and the basic role of the μ^- in these processes can be understood by considering it to be a heavy electron with a mass ratio m_μ/m_e of 207. Therefore, in order to understand the physics of μCF, the following classification of the processes involved is relevant: (1) nuclear process of the fusion reaction in a muonic molecule; (2) intermediate processes of muon sticking and regeneration; (3) *electromagnetic atomic and molecular processes* of muonic atom formation / intra-atomic cascade and slowing-down, muon transfer among hydrogen isotopes, formation of a muonic molecule / intra-molecular transition, and the He impurity effect in μCF involving hydrogen isotopes.

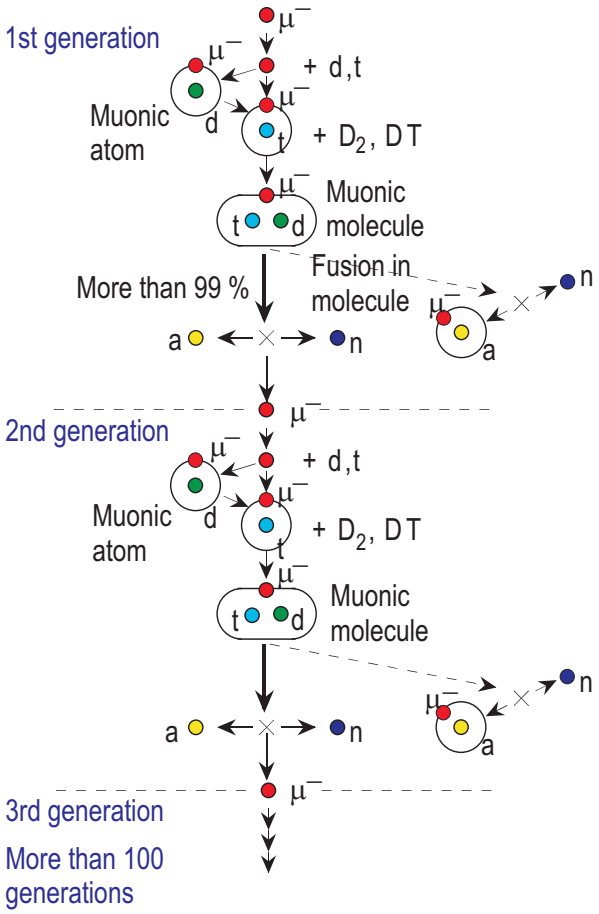

Fig. 11.6. The μCF chain reaction in a D-T mixture.

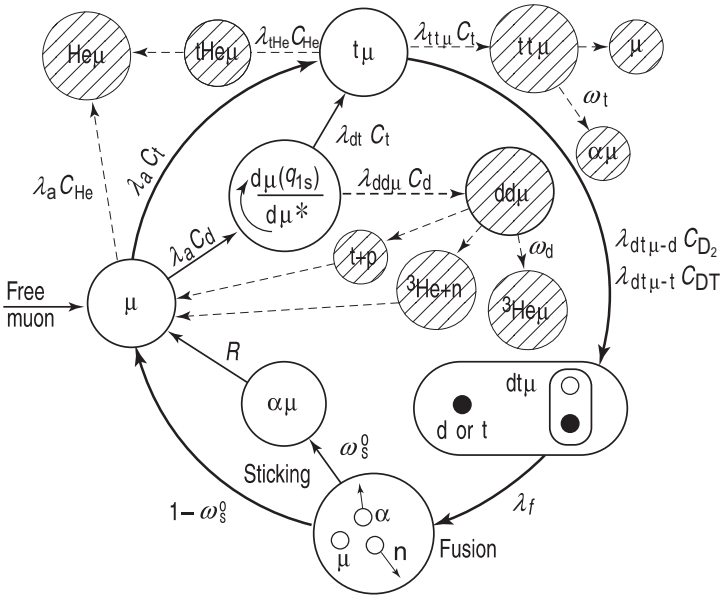

Fig. 11.7. Cyclic representation of the μCF chain reaction in a D-T mixture, including the hyperfine effect and possible energy-loss processes other than (αμ) sticking.

The concept of μCF was introduced independently from another by Frank [47Fra] and Sakharov [48Sak]. An experimental observation of H-D μCF was made by Alvarez et al. at Berkeley [57Alv]. The major historical trends in μCF studies are summarized in Table 11.5. Several review articles are available on the topic of μCF phenomena [89Bre, 89Coh, 90Pon, 92Pet, 92Fro, 98Nag], as well as Proceedings of regular international conferences [87Nag2, 88Vor, 89Jon, 90Bre, 93Fro, 96Pon, 99Pet1, 99Pet2, 02Ish].

Let us summarize the basic important features in favor of μCF as a possible source of fusion energy: (1) Similar to other fusion techniques such as thermo-nuclear or inertial fusion, μCF is a clean energy source without considerable problems of fuel supply; (2) μCF does not need high temperatures; (3) since it is initiated by the operation of an accelerator, μCF is a fully controlled energy source without any phenomenon of criticality.

Table 11.5. Major historical trends of μCF studies.

1947	Hypothesis of the μCF cycle (Frank)
1948	Estimate of the fusion rate λ_f^{dd} (Sakharov)
1956	Observation of (pdμ) fusion (Alvarez)
1957	Calculation of the (dtμ) cycle and sticking (Jackson)
1966	Observation of the T-dependence of $\lambda_{dd\mu}$ (Dzhelepov)
1967	Hypothesis of the resonant formation of (ddμ) (Vesman)
1977	Prediction of large $\lambda_{dt\mu}$ (Gerstein and Ponomarev)
1979	Observation of upper limits on $\lambda_{dt\mu}$ and λ_{dt} (Dubna)
1979	Observation of the hyperfine effect in $\lambda_{dd\mu}$ (PSI)
1982	Measurement of $\lambda_{dt\mu}$, λ_{dt} (LAMPF)
1986	Observation of three-body effect in $\lambda_{dt\mu}$ (LAMPF, PSI)
1987	Observation of X-rays from $(\mu\alpha)^+$ in D-T μCF (PSI, KEK)
1987	Observation of X-rays from (dHeμ) (KEK)
1993	Observation of a large $\lambda_{dd\mu}$ in solid D_2 (TRIUMF)
1994	Observation of X-rays from muon transfer (PSI, KEK)
1995	Observation of $\lambda_{dt\mu}$ with eV (tμ) (TRIUMF)
1997	Systematic studies of X-rays, neutrons from D-T μCF (RIKEN-RAL)
2001	Measurements of $\lambda_{dt\mu}$ at high T and medium ϕ (Dubna)
	Observation of anomalous T-dependence in $\lambda_{dt\mu}$ and W in solid D-T (RIKEN-RAL)

11.6 Experimental arrangements

Once reasonably intense μ^- beams become available, experiments on muon-catalyzed fusion can be realized with the following arrangements. As described in Sect. 11.3, there are two types of accelerator-produced μ^- beams, either continuous or pulsed. The particles (fusion neutron, fusion protons, α-particle, etc.) or photons emitted during the fusion reaction can be detected with reference to the introduced μ^-. Usually, the electron from a μ^- decay after the fusion cycle can be used either for normalizing the muon-number determination or for identifying muon-related events.

The experimental setup, as depicted in Fig. 11.8, comprises the ending part of the μ^- beam channel, a target chamber and detectors for the decay electrons. Some details of the experimental arrangements for the fusion products as well as the representative μCF experiments are described below with respect to understanding each step of the μCF process.

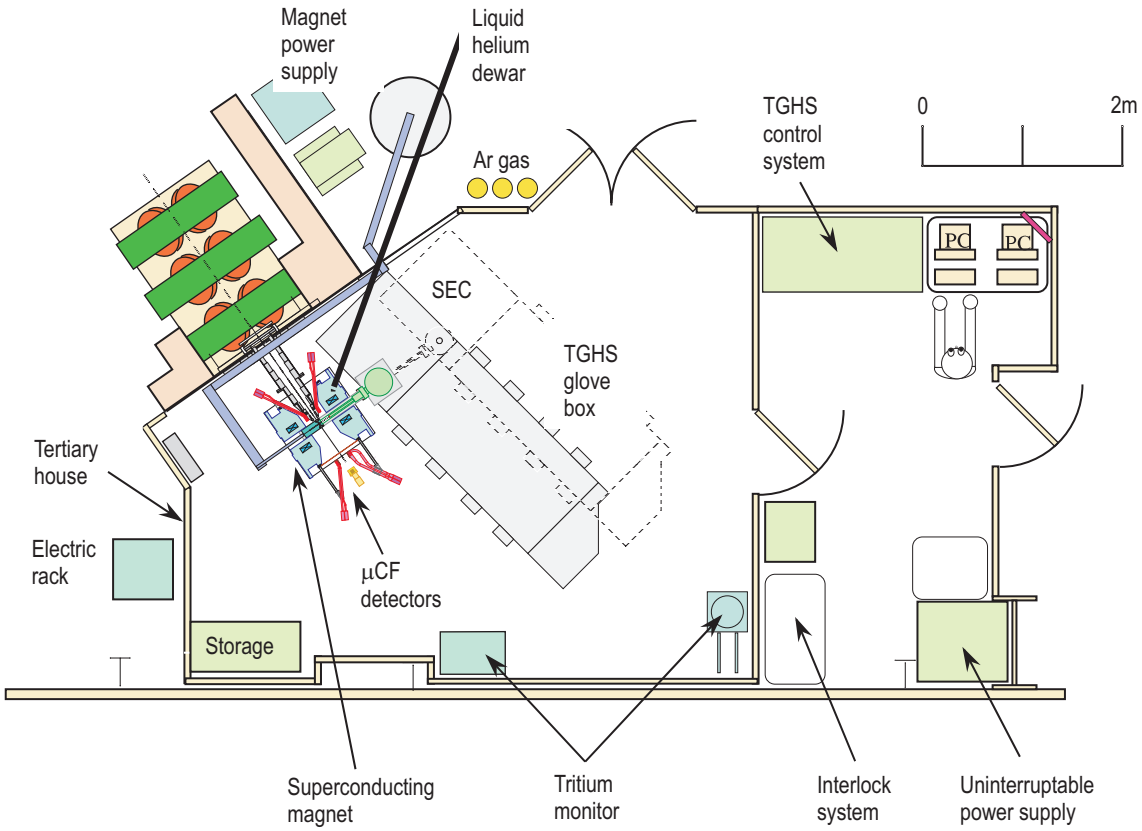

Fig. 11.8. Typical example of an experimental arrangement for μCF studies using a pulsed μ^- beam at RIKEN-RAL [02Mat].

The following remarks concern some detailed specifications of the different detectors, in particular those for fusion neutrons. With the occurrence of the μCF reaction inside the muonic molecule, fusion neutrons are emitted with relatively high energy: 14.1 MeV in (dtμ), ≈ 5 MeV in (ttμ) and 2.5 MeV in (ddμ). The standard neutron counter used is a liquid organic scintillator known under the commercial name *NE213*. In order to eliminate the contribution of radiation background, the method of neutron-γ discrimination, based upon the time-dependent character of the scintillation process, must be employed. The energy calibration as well as the efficiency calibration should be done using standard neutron sources available at the low-energy accelerator facilities. In case of (dtμ), the detection of the fusion neutron is relatively easy because of its high-energy nature. On the contrary, in case of (ddμ), the identification of the neutron signal under huge radiation background is not so easy. Thus, event identification with a coincidence signal from the decay electron is sometimes employed.

The use of a significant amount of radioactive tritium is inevitable in case of D-T μCF studies. The 1 g of pure T_2 (1/6 mols, 3.6 ℓ STP and 10 cm^3 in liquid) corresponds to 10^4 Ci (3.7×10^{14} Bq). Special caution is needed for the handling of radioactive tritium. Usually, as realized at PSI, RIKEN-RAL or Dubna, a special T_2 gas-handling system is required for storage and transport of gas mixtures containing T_2. The layout of the system used at RIKEN-RAL is shown in Fig. 11.9. Moreover, since tritium β-decays produce a ^{3}He impurity at a rate of 100 ppm/day, it is important to install the ^{3}He removal system by employing a Pd filter. As described below, a removal of ^{3}He down to the level of below 100 ppm is required to study μCF phenomena in high-density D-T mixtures. Some descriptions are available for the updated tritium-handling system in use for the current μCF experiment [99Mat, 02Mat, 99Yuk] as well as a summary of the systems used in the past experiments [95Sto].

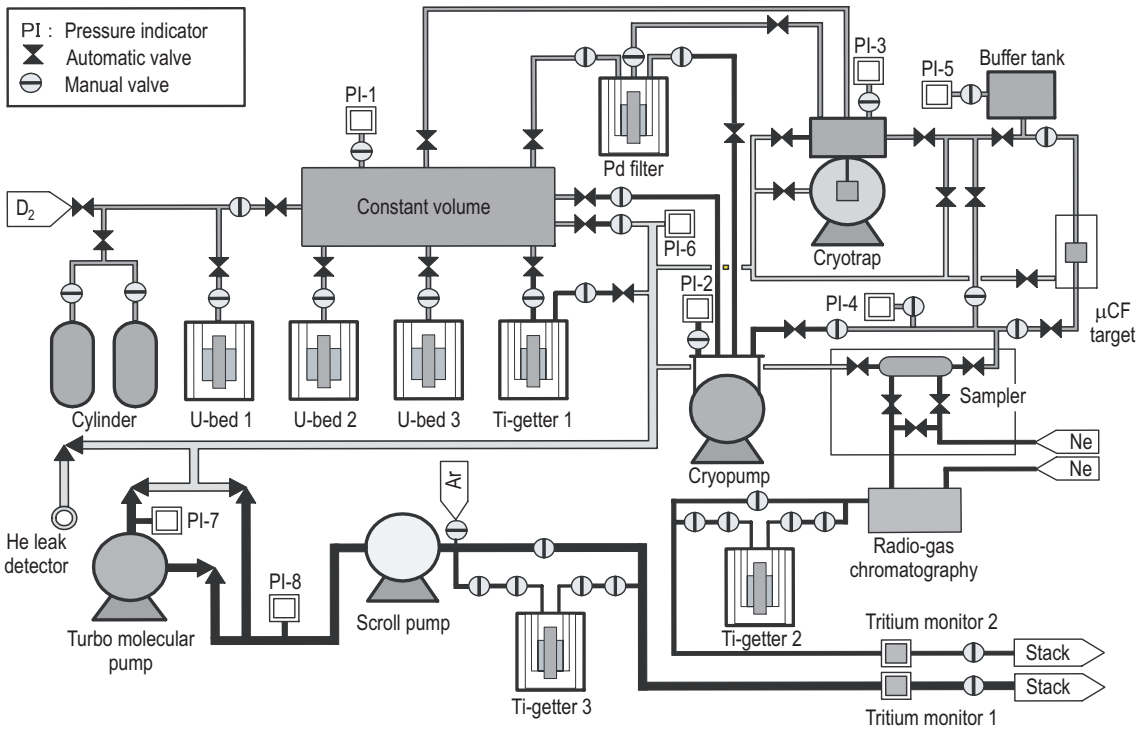

Fig. 11.9. Diagram of the tritium gas-handling system at RIKEN-RAL [02Mat].

11.7 Fusion reaction in a small muonic molecule

Let us now consider how this small (dtμ) molecule looks like. The μ^- in the ground state of muonic hydrogen (μ^-p) is known to have an orbital radius of 260 fm and a binding energy of 2.5 keV. By analogy with the conversion from H(1s) to H_2^+ (ground state), where the radius doubles and the binding energy decreases by a factor of ten, it is reasonable to conclude that the $(pp\mu)^+$ molecular ion has a radius of 2×260 fm and a binding energy of $2.5 \times (1/10)$ keV. The situation is summarized in Fig. 11.10. Thus the size of the molecule does not greatly exceed the range of the nuclear interaction (a few fm) and so, with the help of the zero-point motion of the molecular ion, the fusion reaction proceeds quickly.

Historically, the nuclear fusion rate λ_f inside the small muonic molecule was first calculated using the so-called factorization relations [57Jac], that is,

$$\lambda_f = a_f |\psi(R)|^2, \tag{11.11}$$

where a_f is a reaction constant related to the fusion cross section at zero relative energy (interpolated from the nuclear reaction data at higher energies) and $|\psi(R)|^2$ is the probability density to find the two nuclei at a distance of R. The constant a_f is obtained from the interpolation $v \to 0$ together with a description of the low-energy cross section of the fusion reaction,

$$\sigma = a_f C_0^2 v^{-1}, \tag{11.12}$$

where C_0 is the Gamow factor of s-wave scattering and v is the relative velocity at infinity. From this approach, the result $\lambda_f \approx 10^{12}$ s^{-1} was obtained [57Jac].

There are several shortcomings in factorization treatments of the fusion rate. First of all, we need to know the fusion rate for excited states of the muonic molecule specified by the rotational quantum number (J) and the vibrational quantum number (v) since, as described below, the muonic molecule is formed

in an excited state. Secondly, distortion of the molecular wave function due to the nuclear interaction should be taken into account. Moreover, another correction is needed in the formula for λ_f due to the dominance of a near-threshold resonance in the reaction cross section.

Advanced calculations of the fusion rates at various levels of the muonic molecule (dtμ) were made by Bogdanova et al. [88Bog] and Kamimura [89Kam1, 89Kam2] using the complex nuclear potential (optical potential) method, as well as by Struensee et al. [88Str1, 88Str2], Szalewicz et al. [90Sza] and Hu et al. [94Hu] using the R-matrix method. All four types of calculations gave similar results concerning the fusion rates of the $J = 0$ states of (dtμ), as is summarized in Table 11.6. There, binding energies of (Jv) states of (dtμ) and (ddμ) are also presented. For comparison, fusion rates in the typical muon molecules other than (ddμ) and (dtμ) are summarized in Table 11.7.

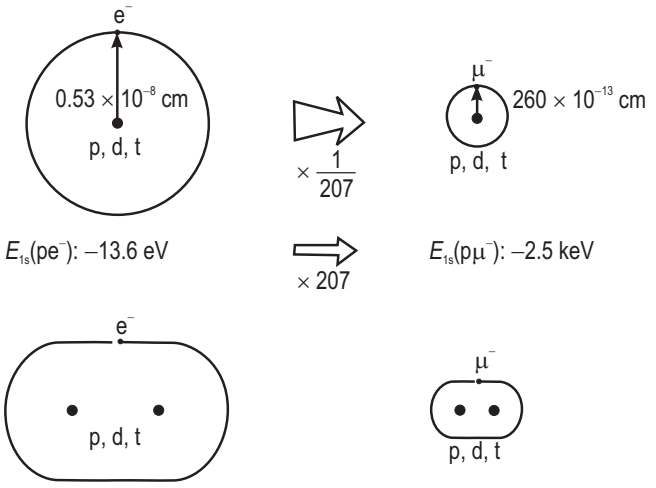

Fig. 11.10. Basic properties of muonic hydrogen and of its molecular ion with reference to the equivalent electronic species.

Table 11.6. Theoretical calculations of muon-catalyzed fusion rates for different quantum states of (dtμ) and (ddμ) molecules, respectively. In addition, the level energies of the quantum states are listed.

State (Jv)	(00)	(01)	(10)	(11)
(dtμ) fusion rate [s^{-1}]				
Bogdanova et al. [88Bog]	1.0×10^{12}	0.80×10^{12}	1.1×10^{8}	4.2×10^{7}
Struensee et al. [88Str2]	1.30×10^{12}	1.13×10^{12}	$(1.32…4.38)\times10^{8}$	$(0.51…1.71)\times10^{8}$
Kamimura [89Kam1, 89Kam2]	$(1.22…1.28)\times10^{12}$	$(1.03…1.08)\times10^{12}$		
Szalewicz et al. [90Sza]	1.25×10^{12}	1.05×10^{12}		
(ddμ) fusion rate [s^{-1}]				
Bogdanova et al. [88Bog]			4.3×10^{8}	1.5×10^{9}

State (Jv)	(00)	(01)	(10)	(11)	(20)
Level energy [eV]					
(dtμ)	319·140	34·834	232·472	0·66017	101·416
(ddμ)	325·074	35·844	226·682	1·97482	86·434

Table 11.7. Theoretical and experimental values of muon-catalyzed fusion rates for typical muon molecules other than (dtμ) and (ddμ). Experimental uncertainties are given in brackets. The level energies of the quantum states are listed as well.

Molecule ($J\nu$)	Reaction channel	Ratio [%]	Theoretical fusion rate [s^{-1}]	Experimental fusion rate [s^{-1}]
(pdμ) (00)	$\mu^3He + \gamma$	86	8×10^5 [a])	
			$9.7(1) \times 10^5$ ($\lambda_{t,\gamma}^{1/2}$) [b])	$3.5(2) \times 10^5$ [c])
			$1.07(6) \times 10^5$ ($\lambda_{t,\gamma}^{3/2}$) [b])	$1.1(1) \times 10^5$ [c])
	$^3He + \mu$	14	$0.62(2) \times 10^5$ ($\lambda_{t,\mu}^{1/2}$) [b])	$0.56(6) \times 10^5$ [d])
(ptμ) (00)	$\mu^4He + \gamma\,(e^+e^-)$	95	1.3×10^6 [a])	$6.5(7) \times 10^4$ [e])
	$^4He + \mu$	5	1.3×10^5	
(ttμ) (11)	$\mu^4He + 2n$	14	1.2×10^7 [a])	
(10)	$^4He + 2n + \mu$	86	1.3×10^7 [a])	1.5×10^7 [f])
($d^3He\mu$) ($J = 0$)			10^2 [g])	
($J = 0$)			$3(1) \times 10^8$ [h])	
($J = 0$)			$6(3) \times 10^5$ [h])	

State ($J\nu$)	(00)	(01)	(10)	(11)	(20)	(30)
Level energy [eV]						
(ppμ)	253·152	–	107·266	–	–	–
(pdμ)	221·549	–	97·498	–	–	–
(ptμ)	213·840	–	99·127	–	–	–
(ttμ)	362·910	83·771	289·142	45·296	172·652	48·813

[a]) Bogdanova [82Bog, 88Bog].
[b]) Friar et al. [91Fri].
[c]) Petitjean et al. [90Pet].
[d]) Bogdanova et al. [90Bog].
[e]) Baumann et al.
[f]) Breunlich et al. [87Bre].
[g]) Kravtsov et al. [84Kra].
[h]) Kamimura [89Kam1, 89Kam2].

In order to understand the overall fusion rate in a muonic molecule, the detailed nature of the intramolecular cascade transitions must be known. As described below, the formation of muonic molecules occurs mostly via a resonant reaction leading to an excited rotational-vibrational ($J\nu$) state with $J = \nu = 1$ which is very weakly bound with respect to the $(t\mu)_{1s} + d$ threshold. The de-excitation of the muonic molecule proceeds via Auger transitions, according to $[(dt\mu)_{J\nu}\, d2e]^* \rightarrow [(dt\mu)_{J'\nu'}\, de]^+ + e$. The rates of these Auger de-excitation processes of the muonic molecule have been theoretically estimated by Bogdanova et al. [82Bog, 82Vin]. In Fig. 11.11, the fusion-reaction rates and the cascade-transition rates for (dtμ) and (ddμ) molecules are summarized.

In case of the (dtμ) molecule, 80 % of the fusion reactions take place from the ($J\nu$) = (01) state and 20 % from the (00) state, both of which are formed after cascading down from the (11) state. Combining all these arguments on the rates of fusion and de-excitation, we can conclude that the fusion reaction is completed in the muonic molecule in a time of 10^{-11} s (corresponding to a rate of 10^{11} s^{-1}) after the formation of the (11) state of the (dtμ) molecule during a collision between (tμ) and D_2.

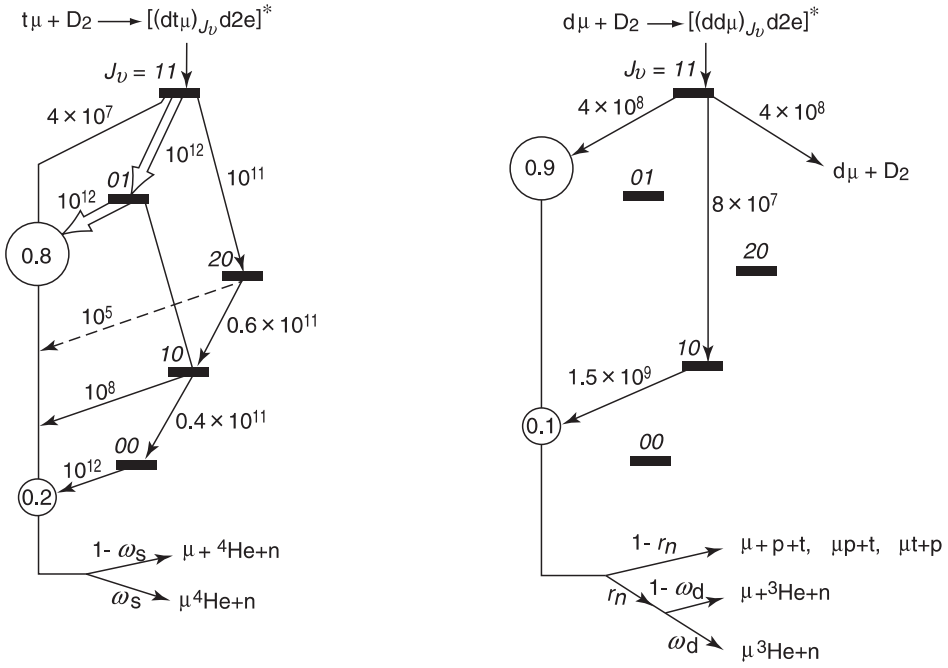

Fig. 11.11. Scheme of cascade processes in (dtμ) and (ddμ) molecules after resonant molecular formation in the (11) state, calculated by Bogdanova et al. [82Bog, 82Vin].

As is also shown in Fig. 11.11, for (ddμ) formed in the $(J\nu) = (11)$ state, the fusion reaction takes place from the (11) and (10) states at a rate of around 10^8 s^{-1}. In this case of identical nuclei, the molecular transition of $J = 1 \rightarrow J = 0$ is suppressed because it would require to change the nuclear spin. Thus, fusion in (ddμ) takes place from the p-wave of relative motion of the nuclei. For (ttμ) fusion, which is listed in Table 11.7, the situation is similar.

The branching ratio of the (ddμ) fusion, $R = N(^3\text{He} + \text{n})/N(\text{t} + \text{p})$, is known to be asymmetric, 1.450 (11) for $J = 1$ [01Vor]. Theoretical understanding was given by Coulomb-corrected R-matrix calculation [90Hal].

11.8 Muonic atom thermalization and muon transfer among hydrogen isotopes

As described in Sect. 11.4, during the cascade process in muonic hydrogen atoms (pμ, dμ, tμ) in a condensed D-T mixture, these atoms are subject to either acceleration or deceleration. Therefore, the history of (dμ) or (tμ) after its formation in a D-T mixture will have the succeeding collision process before or after thermalization, which will be determined by the competition among elastic scattering, the cascade process and other processes like muon transfer from d to t or muonic molecule formation.

Elastic scattering and the competing processes of neutral (dμ) and (tμ) atoms can be quantitatively described by the energy dependence of the cross sections. Originally, the elastic scattering of, e.g., (tμ) was considered to collide with the nucleus of d or t according to

$$(\text{t}\mu) + \text{d} \rightarrow (\text{t}\mu) + \text{d} \,. \tag{11.13}$$

It is possible to make a direct measurement of the cross section for elastic scattering of (dμ) + d using energetic (dμ) available from the Ramsauer-Townsend effect. Suppose that a μ^- is introduced into a solid layer of H_2 containing a small amount of D_2 impurity (around 0.1 %). After the μ^- has stopped and

formed (pμ) atoms, there is some probability for a μ^- transfer reaction from (pμ) to d, producing energetic (dμ) due to the difference in binding energy. In experimental studies the energetic (dμ) was found to be emitted from the surface of the $H_2 + D_2$ layer. These energetic (dμ) can be used to study the elastic scattering process. If a second thin D_2 layer is deposited onto the $H_2 + D_2$ layer, since the (ddμ) fusion takes place at thermalized energies, one can learn, by detection of a fusion product such as, e.g., the 3 MeV proton, the range of (dμ) as a function of the D_2 thickness, and this can in turn be converted into the energy dependence of the elastic scattering of (dμ) + d in solid D_2. The experimental result obtained demonstrates the importance of molecular and/or condensed-matter effects [96Str].

Theoretical studies on the elastic scattering of muonic hydrogen atoms from hydrogen isotopes have been extended to include the molecular effects. Typical theoretical calculations for the elastic scattering of (dμ) from a d nucleus, from a D atom and from a D_2 molecule [88Ada, 89Bra, 89Ada] have been extended to include a condensed-matter effect, where H_2, D_2, T_2 are formed in a liquid or solid [96Ada]. It was shown that in solid matter the phonon spectrum does change the elastic scattering cross section.

In the actual μCF experiments, a condensed phase, such as the liquid or solid phase, is used as well. In experiments with a solid phase of D_2, the thermalization takes a different form compared to that in the gas phase; the thermalization of (dμ) is not completed because of the existence of an "energy gap" in solid D_2 [01Ada]. So far, several pieces of significant evidence exist for a condensed-matter effect on the incomplete thermalization: (1) The π^-p atom at its formation in liquid hydrogen was found to have a kinetic energy from 1 eV to more than 100 eV [91Cra, 97Bad]; (2) as is explained below, recent data concerning muon transfer from excited (pμ) to d can only be explained by the existence of an energetic (pμ); (3) as is again explained below, an energetic (dμ) might explain a large $\lambda_{dd\mu}$ in solid D_2.

As is summarized in the proceedings of μCF̃-01 [02Ish], there exist several theoretical studies which successfully explain production mechanisms of energetic pionic or muonic hydrogen atoms, based upon acceleration mechanisms during the cascade transition.

In a D-T mixture with a density ϕ of around ϕ_0, after injection at MeV energies, it takes 10^{-10} s for the μ^- to reach its ground state of either (dμ) or (tμ). Since the ground-state energy of (tμ) is lower than that of (dμ) by 48 eV, a μ^- initially in a (dμ) atom in its ground state can easily be transferred through the reaction (dμ) + t → (tμ) + d via a collision with t in either T_2 or DT. Since the transfer rate of the μ^- is comparable to the cascade (mainly radiative among low-lying levels) transition rate in (dμ) or (tμ), there is a possibility for the μ^- to undergo a transfer reaction while in an excited state. The probability for the μ^- to reach the ground state before transfer is denoted by q_{1s}, and the problem of excited-state transfer of μ^- is sometimes referred to as the q_{1s} problem [83Pon]; $q_{1s} = 1$ corresponds to μ^- transfer after the μ^- has reached the ground state. Moreover, it has been pointed out that the (dμ) → (tμ) transfer reaction might occur at an epithermal energy with respect to (dμ). Some quantitative arguments related to q_{1s} at various values of C_t, ϕ and E(dμ) are summarized in Fig. 11.12.

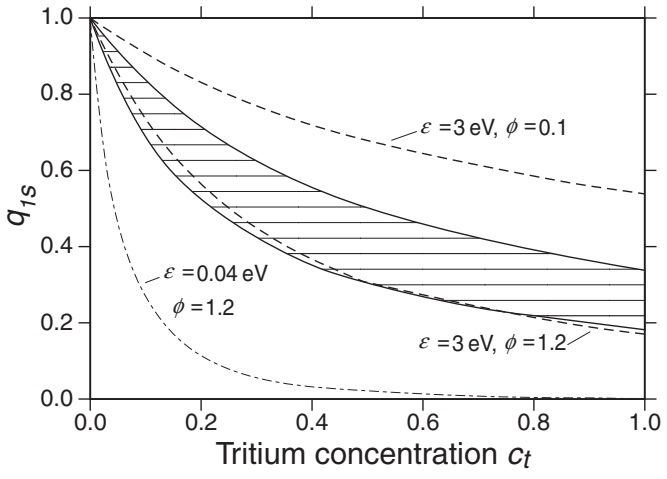

Fig. 11.12. Theoretical prediction of the q_{1s} values in the (dμ) + t → (tμ) + d transfer reaction [96Cza] together with the experimental values extracted from neutron data in (dtμ) μCF, displayed as a function of the tritium concentration C_t at various (dμ) energies ε and densities ϕ [99Ack].

Experimentally, it is possible to measure the value of q_{1s} directly by comparing, e.g., the K_α X-ray energies either of (dμ) and (tμ) for (dμ) to t transfer or of (pμ) and (dμ) for (pμ) to d transfer. Depending upon which X-rays are detected, one can simply conclude whether the transfer occurs from excited states or from the ground state. Such an experiment has become feasible with the development of high-resolution X-ray spectrometers. So far, two experiments have been carried out for the (pμ) to d transfer: (1) using CCDs (charge coupled devices) at PSI [96Lau], and (2) using 7-channel segmented small Si(Li) detectors at KEK-MSL and at RIKEN-RAL [96Sak]. The results have shown the importance of energetic (pμ) for the transfer to d from excited states of (pμ).

Theoretical studies on the transfer reaction among hydrogen isotopes have been carried out and have been extended to cover the q_{1s} problem, as well as the energy-dependence of the initial state and other details. The general tendency for the experimental values of q_{1s} in D-T is to be systematically larger than the theoretical values. This can be accounted for by considering the possible existence of side-paths; the excited (tμ) states formed via transfer reactions from the excited (dμ) states collide with D_2 and resonantly form $(dt\mu)^*$ molecules which mostly decay into $(t\mu)_{g.s.}$ + d. The net result is the apparent formation of additional $(t\mu)_{g.s.}$ [95Fro].

11.9 Formation of muonic molecules

The small neutral (tμ) atom may closely approach a d nucleus in D_2 or DT leading to the formation of a $(dt\mu)^+$ molecular ion, the ground state of which is small in size ($\approx 2a_\mu = 520$ fm) and tightly bound ($0.1\,E_\mu \approx -300$ eV).

Usually, the formation rate of a tightly bound molecular state is relatively low. The most promising way is so-called Auger capture which proceeds according to

$$(d\mu) + D2 \rightarrow [(dd\mu)de]^+ + e^- , \tag{11.14}$$

$$(t\mu) + D2 \rightarrow [(dt\mu)de]^+ + e^- . \tag{11.15}$$

The theoretically predicted formation rate in the ground state is fairly low, of the order of $10^6\ s^{-1}$ (comparable to the μ^- free-decay rate).

However, Gerstein and Ponomarev [77Ger, 79Vin] predicted that an extremely shallow bound state with both the rotational and the vibrational quantum numbers equal to one, i.e. $(Jv) = (11)$, exists at an energy of $\varepsilon_{11} \approx -0.6$ eV, measured from the threshold energy $(t\mu)_{1s}$ + d. One should note that this energy of 0.6 eV is substantially lower than both the ionization energy of the D_2 molecule (≈ 15 eV) and the dissociation energy of the D_2 molecule (≈ 4.5 eV). Due to the existence of this shallow bound state, substantially enhanced formation rates are expected through the following reaction process (known as resonant molecular formation), as is displayed in Fig. 11.13:

$$(t\mu) + D_2 \rightarrow [(dt\mu)_{11}d2e]^* \qquad (\lambda_{dt\mu\text{-}d}), \tag{11.16}$$

$$(t\mu) + DT \rightarrow [(dt\mu)_{11}d2e]^* \qquad (\lambda_{dt\mu\text{-}t}). \tag{11.17}$$

Experimentally, the formation rate of the muonic molecule can be obtained from the relations between the observed overall cycling rate λ_c and the rates of the individual processes, e.g. λ_{dt} and $\lambda_{dt\mu}$, as shown diagrammatically in Fig. 11.14. Let us consider μCF taking place in a D-T mixture with both high density ϕ and high C_t, and further assume that the atomic capture rates and fusion rates are substantially higher than the μ^- decay rate, i.e. $\lambda_{d\mu}, \lambda_{t\mu}, \lambda_f >> \lambda_0$. The inverse of the cycling rate, λ_c^{-1}, then corresponds to the waiting time of (dμ) for muon transfer to t together with the time taken to form the molecule, i.e.

$$\frac{1}{\lambda_c} \approx \frac{q_{1s} C_d}{\lambda_{dt} C_t} + \frac{1}{\lambda_{dt\mu} C_d} , \tag{11.18}$$

where the factor $q_{1s}C_d$ is the probability that the muon reaches the ground state of (dμ), reflecting the fact that the transfer rates from the excited states of (dμ) are very rapid. In most of the D-T μCF experiments

described elsewhere [02Ish], q_{1s} is assumed to be parametrized as $(1 + aqC_t)^{-1}$, and $\lambda_{dt\mu}$ is taken to be $\lambda_{dt\mu}{}^0$, where $\lambda_{dt\mu}{}^1$ is neglected due to theoretical predictions.

In the above formula, λ_c is maximized under the following condition:

$$C_t \approx (1 + \gamma)^{-1}, \quad \gamma = (\lambda_{dt} / q_{1s}\lambda_{dt\mu})^{1/2}. \tag{11.19}$$

In a D-T mixture, the three molecules D_2, DT and T_2 exist with concentrations C_{D_2}, C_{DT} and C_{T_2}, determined by the conditions of chemical equilibrium. Thus, the rate $\lambda_{dt\mu}$ can be decomposed into the sum of two terms,

$$\lambda_{dt\mu} = \lambda_{dt\mu\text{-}d}C_{D_2} + \lambda_{dt\mu\text{-}t}C_{DT} . \tag{11.20}$$

The idea of resonant molecular formation was qualitatively confirmed by the Dubna group in 1979 [81Bys] and in more detail by experiments at Los Alamos [83Jon, 86Jon] and at PSI [87Bre]. In the latter experiments, both the "three-body effects" exhibited in a density dependence of the once density-normalized $\lambda_{dt\mu}$ and a strange temperature dependence in $\lambda_{dt\mu}$ were discovered. At the same time, a very rapid formation rate (of the order of 6×10^8 s^{-1}) was experimentally established for ϕ being close to ϕ_0 for a temperature range up to 800 K. These measurements are summarized in Fig. 11.15 including recent data [99Ack, 03Kaw]. Although not contained in Fig. 11.15, almost consistent data were obtained at Dubna in the range of 300 K $\leq T \leq$ 800 K and 0.25 $\phi_0 < \phi <$ 0.5 ϕ_0 [01Bom]. Theoretical predictions based upon the resonant molecular formation model have not been able to explain the observed temperature dependence of the molecular formation rate; according to theoretical predictions, there should be a steeper decrease in $\lambda_{dt\mu}$ towards the lowest temperature.

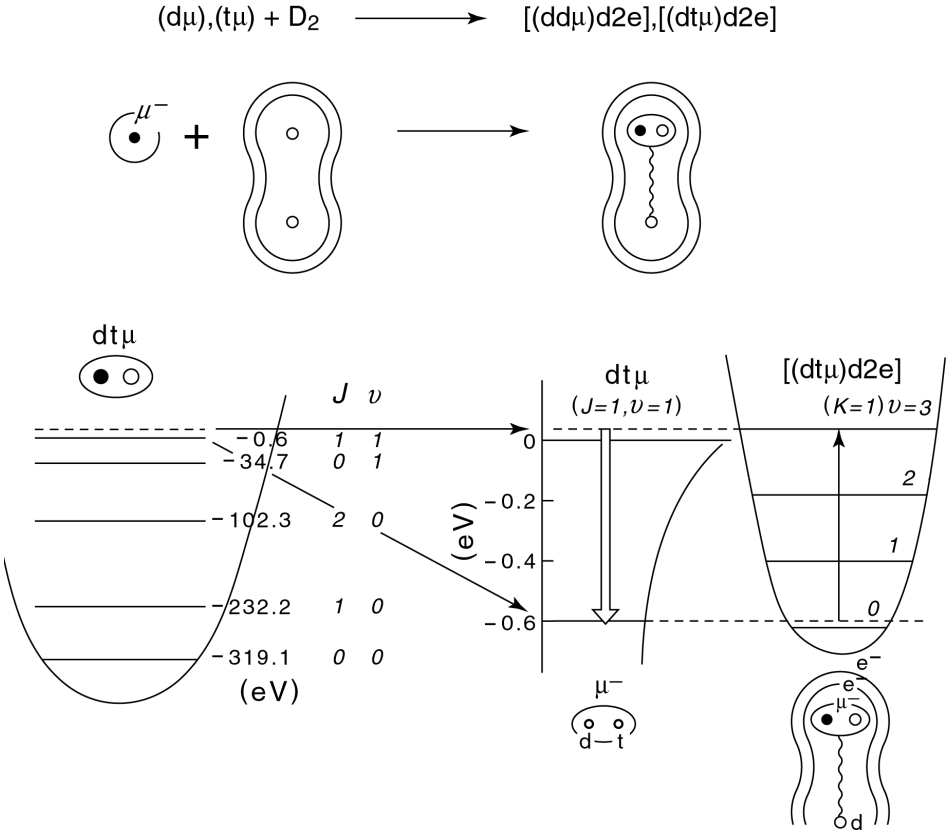

Fig. 11.13. Conceptual view of the resonant molecular formation mechanism of (dtμ) originally proposed [67Ves, 77Ger].

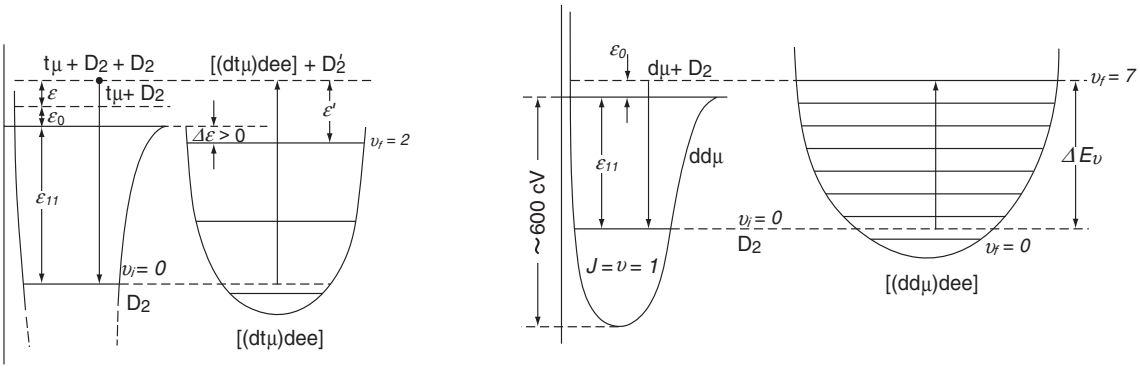

Fig. 11.14. Details of the revised energy-level diagram for resonant molecular formation [90Pon]; (dtμ), where one D_2 molecule, with participation of the other D_2 molecule, is excited to $\nu_f = 2$, versus (ddμ), where the D_2 molecule is excited from ($\nu_i = 2$, $K_i = 2$) to ($\nu_f = 7$, $K_f = 1$).

Experimentally, the existence of "three-body collisions" in $\lambda_{dt\mu\text{-}d}$ has been consistently confirmed. The resonant reaction process between (tμ) and D_2 proceeds under the influence of a second D_2 molecule [86Men], i.e.

$$(t\mu) + D_2 + D_2 \rightarrow [(dt\mu)d2e]^* + D_2 \,. \tag{11.21}$$

Experimental data have shown that such an effect does in fact exist, but only for (tμ) + D_2 and not for (tμ) + DT. At the same time, the phenomenon is effective only for $C_t \geq 0.3$. Assuming $\lambda_{dt\mu} = [\lambda_{dt\mu\text{-}d}^{(1)} + \lambda_{dt\mu\text{-}d}^{(2)}\phi]C_{D_2} + \lambda_{dt\mu\text{-}t}^{(1)}C_{DT}$, the following values (in units of $10^4\ s^{-1}$) were obtained by the Los Alamos experiment [86Jon] at temperatures below 130 K: $\lambda_{dt\mu\text{-}d}^{(1)} = 206(29)$, $\lambda_{dt\mu\text{-}d}^{(2)} = 450(50)$, and $\lambda_{dt\mu\text{-}t}^{(1)} = 23(6)$, where the experimental uncertainties are stated in brackets. The values of $\lambda_{dt\mu\text{-}d}$ and $\lambda_{dt\mu\text{-}t}$ can also be measured directly by employing a non-equilibrium D-T mixture, i.e. $(1-C_t)D_2 + C_tT_2$ before chemical equilibrium among D_2, DT and T_2. Such measurements were performed at Los Alamos [93Jon] and PSI [92Pet].

An accurate calculation of the energy ε_{11} of the $(J\nu) = 11$ state of (dtμ) was one of the main subjects of theoretical studies of muon-catalyzed fusion throughout the 1980s, as is summarized in Table 11.8. There are several corrections to ε_{11} which are larger than 1 meV. These include finite-size nuclear effects, as well as hyperfine effects and energy shifts caused by the host molecule. The total corrections to ε_{11} amount to ≈ +30 meV. For a review of these corrections, see [90Pon].

Theoretical studies are needed for understanding the surprising aspects in the (dtμ) formation rates, namely (a) the strange temperature dependence, and (b) the nonlinear dependence on the mixture density. A theoretical calculation which had been used to calculate the transition-matrix elements in the dipole approximation has been extended to include the quadrupole terms [96Fai]. However, except for a slight reduction of the absolute rate, the explanation of the temperature dependence has not been improved significantly.

Theoretical understanding of the origin of the three-body collision effects has been gained only qualitatively. As suggested in the argument related to Fig. 11.14, in a (tμ) + D_2 collision, a partner is needed to absorb any excess energy for the resonance condition [86Men]. As for the temperature dependence of $\lambda_{dt\mu}$, a phenomenological triple-collision effect was introduced [88Fai], and it was pointed out that low-temperature data could be explained by the (tμ) to (dtμ) transition energy shifting from 0.601 eV to 0.596 eV. Petrov [85Pet1, 85Pet2] has shown how to incorporate the resonance width, while Menshikov et al. [86Men] have developed a theoretical treatment of the formation in triple collisions which includes the effect of the potential from the surrounding molecules on the resonance defect. On the other hand, Leon [89Leo] has developed a model based upon a microscopic multi-step process.

Table 11.8. Historical development of theoretical calculations of the binding energy of $(dt\mu)_{11}$.

Author	Binding energy [eV]	Method
Vinitsky et al. [80Vin]	0.64	adiabatic representation
Gocheva et al. [85Goc]	0.654	adiabatic representation
Vinitsky et al. [86Vin]	0.6589	elliptic-basis variational method
Korobov et al. [87Kor]	0.65968	elliptic-basis variational method
Szalewicz et al. [87Sza]	0.66001	Hylleraas-basis variational method
Kamimura [88Kam]	0.660104	Gaussian-basis in Jacobian coordinate
Monkhorst et al.[88Ale]	0.660172	Slater-geminals-basis variational method

Recent experiments involving simultaneous X-ray and neutron measurements on μCF in high-density, high-C_t D-T mixtures at RIKEN-RAL have produced important new insights concerning the formation mechanism of (dtμ). The results can be summarized as follows:

(1) The density dependence, which had been observed in the gas-phase liquid-phase region ($\phi = 1.2$), seems to exist in the liquid-solid region ($\phi = 1.5$) as well. Results from D-T mixtures with $C_t = 0.28\ldots0.70$ (Fig. 11.15) suggest that the triple-collision effect on $\lambda_{dt\mu}$ coexists with condensed-matter effects in dense phases.

(2) The effect of ^{3}He accumulation in the D-T mixture, which has been observed to be significant in solids but not in liquids [99Kaw], must be corrected before theoretical interpretations of $\lambda_{dt\mu}$.

(3) In systematic studies on μCF in solid D-T mixtures under a variety of conditions, i.e. tritium concentrations from 20 % to 70 % and temperatures from 5 K to 16 K, an increase in the muon cycling rate, λ_c, was observed with increasing temperature. The changes observed seem to be consistent with the temperature dependence of $\lambda_{dt\mu}$ as predicted by the phenomenological triple-collision effect [03Kaw].

In (dtμ) formation, the lowest accessible vibrational transition lies below the threshold (as shown in Fig. 11.13, the kinetic energy of the collision partner would have to be negative to reach a resonance condition). The strongest resonant contributions to molecular formation are due to higher vibrational and rotational transitions, which correspond to kinetic energies of the collision partners of several hundred meV. In a triple mixture of H/D/T, three types of resonant reactions are possible:

$$t\mu + D_2 \rightarrow [(dt\mu)dee] , \tag{11.22}$$

$$t\mu + DT \rightarrow [(dt\mu)tee] , \tag{11.23}$$

$$t\mu + HD \rightarrow [(dt\mu)pee] . \tag{11.24}$$

The rates of these reactions were calculated by Faifman et al. [91Fai, 96Fai] for the initial states of $(t\mu)_{F=0,1}$ and a collision energy of $E \leq 2$ eV. The fast muonic atoms (tμ) realize the above three reactions with the high rate of 10^9 s^{-1} at energies of the (tμ) atoms of $E = 0.2\ldots0.5$ eV before thermalization. The kinetics which take place in the triple mixture H/D/T were extensively studied using Monte Carlo simulations by Markushin et al. [92Mar, 93Mar, 96Mar2].

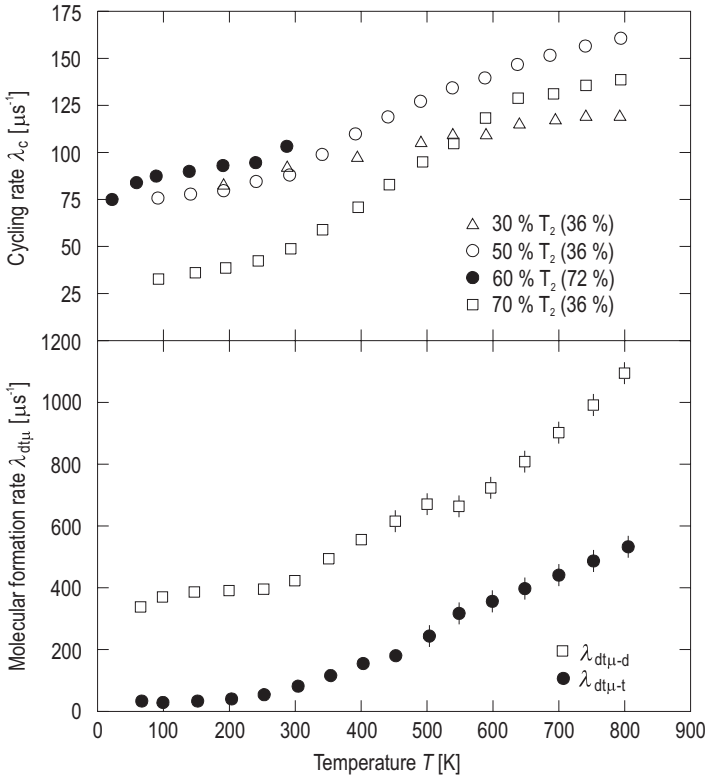

Fig. 11.15. Cycling rate, λ_c, and molecular formation rate, $\lambda_{dt\mu}$, of D-T μCF versus temperature, T.

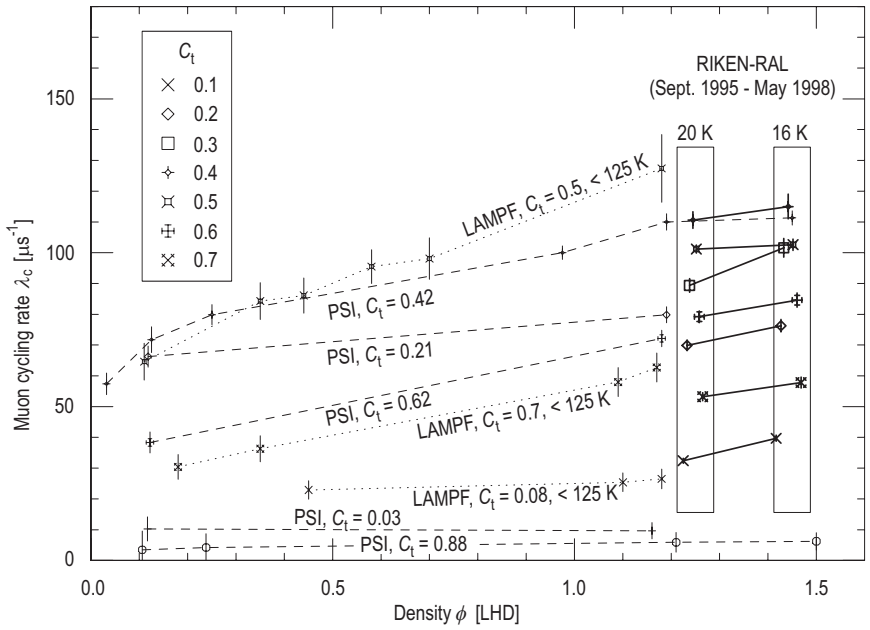

Fig. 11.16. Muon cycling rate, λ_c, of D-T μCF versus density, ϕ.

The understanding of muonic molecular formation can be somewhat extended by consideration of energetic (tμ) or (dμ). The cross section for (dtμ) formation has been theoretically calculated for various (tμ) energies and various energies (temperatures) of D_2 [91Fai, 96Fai]. At high energies, several significant resonances occur; for instance, (tμ) exhibits a strong resonance at 0.1 eV. An enhanced cross section for (dtμ) formation can be expected compared to the cross section for elastic scattering. This leads to the slowing down, and so there is a possibility for resonances of this kind to be detected experimentally. An experiment utilizing the Ramsauer effect in H_2 + 0.1 % T_2 to generate an energetic (tμ) beam was carried out at TRIUMF [96Mar1, 00Fuj, 01Por].

Compared to the formation of (dtμ), the formation of (ddμ) is quantitatively explained by theoretical calculations. Actually, the idea of resonant molecular formation was originally suggested by Vesman in relation to the enhanced (ddμ) formation rate [67Ves], and the resonant formation process is sometimes referred to as Vesman mechanism. Thus, overall agreement between theory and experiment has been achieved for D_2 μCF but is not yet complete for D-T μCF. This general tendency can be qualitatively explained by considering the energy balance between the resonating muonic molecular state and the hydrogen molecule state. As depicted in Fig. 11.14, an energy deficiency exists for D_2 μCF, while an energy excess exists for D-T μCF, so that one more collision partner is needed to take away the excess energy, which is consistent with the picture of triple collisions mentioned above.

In case of D_2 μCF, the ground state of (dμ) has two hyperfine states, $F = 3/2$ and $F = 1/2$, and inelastic hyperfine transitions take place like $(d\mu)(F = 3/2) + d \leftrightarrow (d\mu)(F = 1/2) + d$. Because of a spin dependence in the (ddμ) molecular formation rate, $\lambda_{dd\mu}{}^F$, the hyperfine transitions can be observed in a time-dependent change of fusion neutrons [83Kam]. The intra-molecular transition rate and the fusion rate after the initial ddμ formation in the (1, 1) state are relatively slow so that the back-decay process ($[(dd\mu)d2e] \rightarrow d\mu + D_2$) does compete with them. The temperature dependence in $\lambda_{dd\mu}{}^F$ is perfectly reproduced by the theory of resonant-molecular formation from below 200 K down to 25 K (liquid). As shown in Fig. 11.17, the measured (dμ) spin-dependent formation rate is quite consistent with theory down to the liquid phase. There, the hyperfine transition rate of $(d\mu)_{3/2} \rightarrow (d\mu)_{1/2}$ was also measured, but is inconsistent with theory [01Vor].

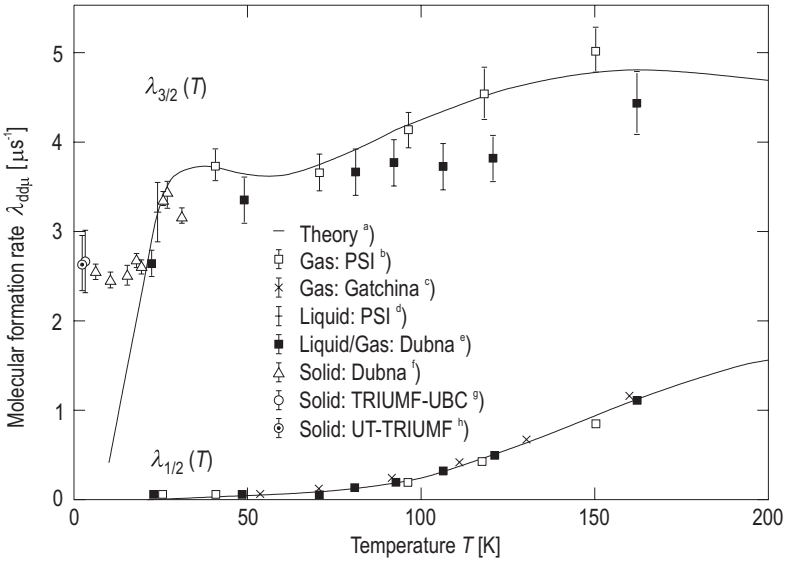

Fig. 11.17. Molecular formation rates $\lambda_{dd\mu}{}^{(3/2)}$ and $\lambda_{dt\mu}{}^{(3/2)}$ measured in gaseous, liquid and solid D_2, together with the corresponding theoretical predictions for gaseous and liquid D_2.
[a]) [93Scr]
[b]) [90Zme]
[c]) [84Bal]
[d]) [89Nae]
[e]) [92Dzh]
[f]) [96Dem]
[g]) [96Kno]
[h]) [96Str]

As for the well-understood (ddμ) formation rate in D_2 μCF above 20 K, it was found that there is a marked deviation of the experiment from the theory below 20 K, corresponding to μCF in the solid phase [96Dem, 96Kno], as is summarized in Fig. 11.17. The deviation is likely to originate from one or both of the following two mechanisms: (a) owing to a non-thermalization effect during the slowing-down of (dμ), the existence of an energy gap in solid D_2 suppresses complete slowing-down, producing non-thermalized epithermal (dμ) (with energy ≈ 20 K); (b) the reaction mechanism of the resonant molecular formation process is dramatically changed because of a change in the final-state energy spectrum, where solid-state effects are taken into account [01Ada].

As pointed out in theoretical calculations [93Scr], below room temperature the resonant formation of (ddμ) proceeds mainly via a process of $(d\mu)_{3/2}$ and D_2 (K_i=0) → D_2 (K_f=1). By controlling low-lying states of the D_2 molecule, ortho (K_i=0, I=0, 2) para (K_i=1, I=1) D_2 with an energy difference of 86 K, one can expect a significant change in the formation rate of (ddμ). Theoretical calculations were made [85Leo, 00Fai] predicting an enhanced $\lambda_{dd\mu}$ below 50 K for pure ortho D_2. Experimental investigation was done in solid D_2, demonstrating the importance of a solid effect in $\lambda_{dd\mu}$ [01Toy, 03Toy].

Similar and much larger effects are predicted for $\lambda_{dt\mu}$, where suppressed (K_i=1) → (K_f=3) is expected for ortho D_2 and enhanced for para D_2 at low temperatures [85Leo, 00Fai].

It is interesting to point out that there seems to be a clear difference between $\lambda_{dd\mu}$ and $\lambda_{dt\mu}$ in their apparent behaviour at low temperatures; the resonance formation of (tμ) + D_2 is a thermalized reaction, while that of (dμ) + D_2 is a non-thermalized reaction.

As summarized in the review article by Ponomarev [90Pon], the formation rates in systems other than (dtμ) or (ddμ) are mostly due to a non-resonant formation process of rotational-vibrational states (Jv). The respective theoretical values are on the whole consistent with the experimental data, as presented in Table 11.9.

Table 11.9. Comparison of experimental and theoretical formation rates.

Molecule	(Jv)	Theoretical rate [10^6 s^{-1}]	Experimental rate [10^6 s^{-1}]
(ppμ)	(10)	2.2	2.5
(pdμ)	(10)	5.9	≈ 6
(ptμ)	(10)	6.5	–
(ttμ)	(11)	3.0	2

11.10 Muon sticking and regeneration in the μCF cycle

To date, a variety of experimental methods has been adopted in order to investigate μCF phenomena in D-T mixtures. Measurements of the 14 MeV fusion neutrons can be used to obtain the fusion-neutron yield, the μCF cycling rate and other parameters, usually with a simultaneous measurement of the decay e^- for normalization purposes. Measurements of the characteristic X-rays corresponding to various processes in the μCF cycle can also provide very valuable insights concerning these processes. Time-dependent measurements of the fusion neutrons and of characteristic X-rays from muonic atoms or molecules can reveal the time evolution of μCF phenomena. A combination of experimental methods may be the optimum approach to obtain satisfactory information about each process of the μCF cycle of Fig. 11.7.

Here we summarize the relationship between experimental observables and physical parameters, in particular the cycling rate λ_c of the μCF cycle, with its accompanying loss probability W accommodating muon-to-alpha sticking phenomena of the μCF cycle.

(1) Neutron method: measurements of the absolute yield Y_n and disappearance rate λ_n (the rate of the time-dependent decrease of the fusion-neutron intensity) give us the loss rate W_n seen by neutrons, thus providing some limiting factor on ω_s:

$$Y_n(t) = \phi \lambda_c e^{-\lambda_n t} , \tag{11.25}$$

$$Y_n = \phi \lambda_c / \lambda_n , \tag{11.26}$$

where $\lambda_n = \lambda_0 + \lambda_c W_n$ and $W_n = \omega_s$ + other losses.
(2) X-ray method: measurements of X-rays from $(\mu\alpha)^+$ ions provide information directly related to sticking phenomena,

$$Y_x(t) = \phi \lambda_c \kappa \omega_s^0 e^{-\lambda_n t} , \tag{11.27}$$

$$Y_x = \phi \lambda_c \kappa \omega_s^0 / \lambda_n , \tag{11.28}$$

where κ, given by the theory of the atomic processes of the $(\mu\alpha)^+$ ion, is the X-ray yield per sticking, and ω_s^0 is the initial sticking probability immediately after the fusion reaction in the muonic molecule.

Combining $Y_x(t)$ and $Y_n(t)$ leads to a direct measure of ω_s^0:

$$Y(K_\alpha, K_\beta, \ldots) = Y_x / Y_n = \kappa(K_\alpha, K_\beta, \ldots)\omega_s^0 . \tag{11.29}$$

Actually, ω_s^0 is the sum of initial sticking contributions corresponding to each orbital of the $(\mu\alpha)^+$ ion,

$$\omega_s^0 = \Sigma_{n\ell}\ \omega_s^0(n\ell) . \tag{11.30}$$

The ω_s which appears in the total loss probability W_n is obtained by correcting ω_s^0 with the regeneration factor R,

$$\omega_s = \omega_s^0 (1-R). \tag{11.31}$$

Again, since the regeneration process depends upon the initial state of the $(\mu\alpha)^+$ ion, ω_s^0 should be written as

$$\omega_s^0 = \Sigma_{n\ell}\ [1-R(n\ell)]\ \omega_s^0(n\ell). \tag{11.32}$$

The experimental values so far obtained from the loss rate W_n seen in the neutron method are summarized in Fig. 11.18 where values of the effective sticking, ω_s, are presented as a function of the density ϕ.

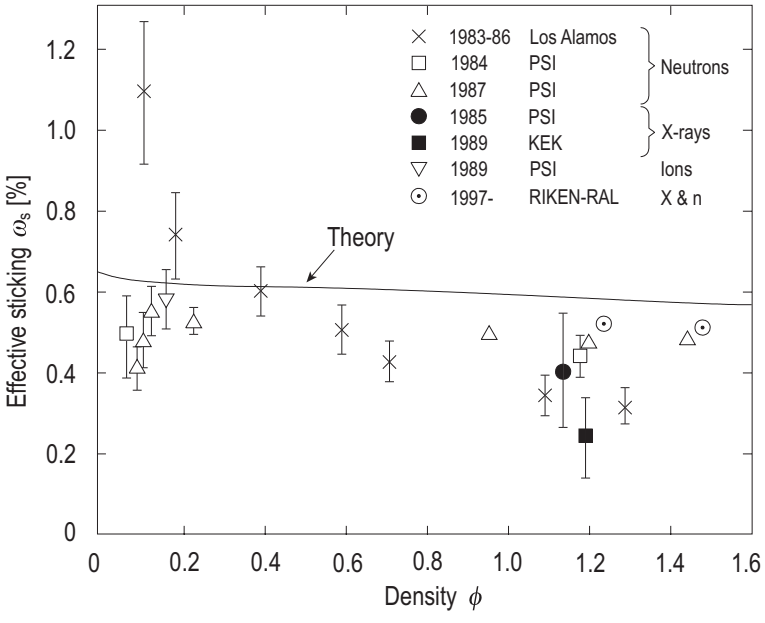

Fig. 11.18. Existing data concerning the sticking probability ω_s versus the density ϕ in muon-catalyzed fusion in a D-T mixture.

Theoretical studies of α-sticking were initiated by Jackson [57Jac] employing the sudden approximation. The probability of $(\mu\alpha)^+$ atom formation in an $n\ell$ state is given by

$$\omega_s^0(n\ell) = \Sigma_m \, |F(n\ell m)|^2 \,, \tag{11.33}$$

$$\text{where } F(n\ell m) = \int \psi_{n\ell m}^*(\boldsymbol{r}) \, e^{i\boldsymbol{q}\cdot\boldsymbol{r}} \, \psi_{in}(\boldsymbol{r}) \, d\boldsymbol{r} \,, \tag{11.34}$$

with $\psi_{n\ell m}(\boldsymbol{r})$ being the wave function of $(\mu\alpha)_{n\ell m}$, and $q = mv$ (v denotes the velocity of $(\mu\alpha)$). In this expression, $\psi_{in}(\boldsymbol{r})$ is the normalized muon wave function at the instant of fusion and can be expressed in terms of the muon-molecule wave function, $\psi_{in}(\boldsymbol{r}, \boldsymbol{R})$, as $\psi_{in}(\boldsymbol{r}) = N\psi_{Jv}(\boldsymbol{r}, \boldsymbol{R} = 0)$, where $\boldsymbol{R}$ is the internuclear distance, $\boldsymbol{r}$ is the muon coordinate with respect to the center of mass of the two nuclei, and N is a normalization constant.

At the earliest stage of the theoretical studies, the initial muon wave function $\psi_{in}(\mathbf{r})$ was simply taken from the μ^- in the $(\mu^5\text{He})$ atom (Born-Oppenheimer approximation), which results in $\omega_s^0 = 1.2$ %. In papers after 1985, the non-adiabatic motion of the muon in the $(dt\mu)$ molecule was taken into account. New methods to solve the Coulomb three-body problem non-adiabatically include a Green-function Monte Carlo method [85Cep], the adiabatic representation method [86Bog], variational methods with a Hylleraas basis [86Hu, 88Hay] and the Jacobian-coordinate coupled-channel method [89Kam1, 89Kam2]; values of ω_s^0 calculated from these three-body wave functions are listed in the upper half of Table 11.10. The non-adiabatic nature of the $(dt\mu)$ wave function reduces the initial sticking by some 25 %.

The effect of the nuclear d-t interaction on the sticking was then studied using the nuclear optical-potential model [89Kam1, 89Kam2, 89Bog] and with R-matrix theory [91Jez, 96Coh]. In the former method, the nuclear d-t potential is directly added to the Coulombic Hamiltonian in order to examine the change in the muon wave function at the nuclear coalescence. In the latter method, the effect of the nuclear interaction is indirectly included by imposing an appropriate nuclear boundary condition on the $(dt\mu)$ wave function at the channel radius. Both methods gave similar results, as shown in the lower half of Table 11.10; the nuclear-interaction effect increases the initial sticking by 3 %.

Table 11.10. Theoretical values of the initial muon sticking probability, ω_s^0 [%], for different (Jv) states of the $(dt\mu)$ molecule, with and without nuclear interaction, respectively.

Author	(Jv) state	
	(00)	(01)
(without nuclear interaction)		
Hu [86Hu]	0.897	0.8649
Ceperley Alder [85Cep]	0.895	
Bogdanova et al. [86Bog]	0.846	0.848
Haywood et al. [88Hay]	0.886	0.888(2)
Kamimura [89Kam1, 89Kam2]	0.8859	0.8896
(with nuclear interaction)		
Bogdanova et al. [89Bog	0.93	
Kamimura [89Kam1, 89Kam2]	0.925(4)	0.927(4)
Jezioski et al. [91Jez]	0.917	0.915
Cohen et al. [96Coh]	0.912	0.913

In order to investigate the nuclear-interaction effect beyond the sudden approximation, Kamimura [87Kam] formulated a four-body $(t + p + n + \mu)$ model of the fusion, $t + (pn) \rightarrow (tp) + n$, and investigated the initial sticking problem starting with fundamental reaction theory. The sudden approximation is equivalent to the so-called zero-range plane-wave Born approximation (PWBA) in reaction theory. In order to greatly improve the part of PWBA, he formulated the zero-range coupled-channel Born approximation (CCBA), which includes, as effects of the strong n-α interaction, the distortion of the plane wave

and coupling among the n-$(\alpha\mu)_{n\ell}$ channels ($n\ell$ includes the continuum states). By this formulation it was found that the final-state-interaction effects do change the absolute value of the transition matrix to each $(\alpha\mu)_{n\ell}$ state, but, as long as the excitation energies of the $(\alpha\mu)_{n\ell}$ states are safely negligible compared with the fusion energy of 17.6 MeV, the change in the transition matrix is independent of the (αμ) states, including the continuum. This means that the initial sticking ω_s^0 does not change since it is the ratio of the transition strength to the bound state of (αμ) to that to all states, including the continuum. Furthermore, from the structure of the transition matrix, the release of the zero-range approximation of the transition interaction does not seem to significantly change that ratio for the calculation of ω_s^0. This prediction [87Kam] was realized afterwards in some efforts to improve the sudden approximation [82Bog, 96Mel]. Another remaining and meaningful improvement of the initial-sticking calculation will be to replace the initial (dtμ) wave function by (dtμ) + (αnμ), for which the Hamiltonian with a nuclear (dt)-(αμ) coupling interaction is diagonalized within the L^2-integrable basis function [89Kam1, 89Kam2].

By adopting the value of the initial sticking probability in Table 11.10, several authors [87Coh, 88Mar, 90Sto] calculated the effective sticking ω_s, taking into account all of the processes involved in the regeneration of the muon from the (αμ) atom, such as Coulomb excitation and de-excitation, Auger transitions, Stark mixing, muon transfer, ionization and radiative de-excitation. As listed in Table 11.11, from the values of R at $\phi = 1.2\phi_0$, one can obtain $\omega_s \approx 0.6$ %. The density-depending theoretical values of ω_s in (dtμ) μCF appear to be consistently higher than the experimental values; in terms of the effective sticking, theoretical calculations predict $\omega_s \approx 0.6$ % while experiments report $\omega_s \approx 0.5$ % as seen in Fig. 11.18. After several trials, the gap has not been filled so far. This is one of the most important problems to be solved in μCF studies. Clearly, a lower value of ω_s increases the number of fusion cycles catalyzed by the muon.

Since 1986, X-ray measurements were applied several times for a direct measurement of the μ-α sticking probability in D-T μCF. As for X-ray detection in (dtμ) μCF, the radiation background due to bremsstrahlung associated with tritium beta-decay is serious; this background, the energy range of which extends up to 17 keV, masks all the ω_s-related X-rays ($E(K_\alpha) = 8.2$ keV, $E(K_\beta) = 9.6$ keV, etc.). The use of pulsed muons is helpful here; by operating the detection system only in a short time interval around each muon pulse, a significant improvement in the signal-to-noise ratio can be obtained. An experiment at PSI [87Bos] was performed with continuous muons upon a low-C_t ($\approx 10^{-4}$) D-T mixture, while those at KEK-MSL [87Nag1, 90Nag] and RIKEN-RAL [98Nag, 02Ish] were carried out with pulsed muons and employed high-C_t mixtures.

Table 11.11. Theoretical predictions of the X-ray intensity and the regeneration factor for (αμ) in D-T μCF. $Y(K_\alpha)$ is the yield of K_α X-rays from $(\mu\alpha)^+$ formed by the muon sticking in dtμ-μCF normalized by the yield of fusion neutrons ("photon/fusion"), $\kappa(K_\alpha)$ is the theoretical prediction of the K_α X-ray intensity per initial sticking ω_s^0 ("photon/sticking"), and R is the regeneration factor representing a fraction of μ^- production of the initial sticking ω_s^0.

Author	$Y(K_\alpha)$ [%] [a])	$\kappa(K_\alpha)$	R [b])	$\frac{(1-R)}{\kappa}$	$\frac{Y(K_\beta)}{Y(K_\alpha)}$ [b])
Cohen [87Coh]	0.25	0.28	0.35(5)	2.3	0.12
Markushin [88Mar]	0.25	0.28	0.35	2.3	0.12
Takahashi [87Tak]	0.24	0.27	0.30	2.6	0.18
Struensee [88Str1]	0.27	0.30	0.35	2.2	0.12
Rafelski [89Raf]	0.30	0.34	0.36	1.9	0.07
Stodden [90Sto]	0.30	0.34	0.34(3)	1.9	0.081

[a]) For $\omega_s^0 = 0.886$ % and $\phi = 1.2\phi_0$.

[b]) For $\phi = 1.2\phi_0$.

Following the first successful observation of K_α X-rays from $(\mu\alpha)^+$ in high-ϕ, high-C_t ($C_t = 0.3$) D-T mixtures at KEK-MSL, the first systematic data on both ω_s and $Y(K_\alpha)$ were subsequently obtained in high-density ($\phi = 1.2\ldots1.5$), high-C_t ($C_t = 0.1\ldots0.7$) D-T mixtures at RIKEN-RAL (Fig. 11.19). The experimental results provided values for (a) the effective sticking probability, ω_s, obtained from fusion-neutron data (after correction for all the other loss processes such as those in (ddμ) and (ttμ)), and (b) the K_α X-ray yield, $Y(K_\alpha)$ (photon/fusion), of the recoiling $(\alpha\mu)^+$ ion formed after a μ^--to-α sticking process.

In Fig. 11.19, the results on ω_s and $Y(K_\alpha)$ are summarized and compared with the corresponding atomic-process calculations [88Str1, 88Str2, 88Mar]. Here a theoretical value of $\omega_s^0 = 0.912$ % [94Hu] for the initial sticking probability was used. It can be seen that the ω_s obtained is smaller than any theoretical value published so far, while the discrepancy in the (αμ) X-ray yield seems to be less significant. In addition, the measured $Y(K_\beta)/Y(K_\alpha)$ values (0.075±0.010 for liquid, 0.060±0.012 for solid [00Nak]) are much smaller than the calculated values (≈ 0.12) with correct Stark mixing at $n = 3$.

The result indicates that either the initial sticking probability should be smaller ($\omega_s^0 \approx 0.75$ %) if we believe the atomic process calculation. Another possible explanation is, if we believe the ω_s^0 calculation, that the atomic process of $(\alpha\mu)^+$ ions has to be reconsidered to explain ω_s, $Y(K_\alpha)$ and $Y(K_\beta)/Y(K_\alpha)$ consistently. Considering the smallness of the observed K_β/K_α intensity ratio, it is likely that the excitation rates from the $n \geq 3$ levels are higher than calculated. This would lead to a smaller ω_s, while $Y(K_\alpha)$ would not be much affected. Thus, although there have been no quantitative explanations, the existence of "anomalous" regeneration (ionization of the recoiling $(\alpha\mu)^+$ ion) has been experimentally observed in high-density, high-C_t D-T mixtures.

Experimental investigations were made at RIKEN-RAL on μCF in solid D-T with $C_t = 0.40$ in the temperature range from 5 K to 20 K [03Kaw]. A significant change was found in the ω_s seen by a loss of the fusion neutron (Fig. 11.19). Based upon observations of no change of X-ray data (photon/fusion), the origin of the observed change can be related to R against temperatures; small ω_s (0.42) and large R at 16 K, while larger ω_s (0.61) and smaller R at 5 K both of which are rather consistent with theories. This anomalous regeneration is an interesting objective for further theoretical investigation. At the same time, it may encourage the development of an idea for the enhancement of energy production in D-T μCF. The result suggests that an even smaller ω_s with larger R can be expected in a high-temperature solid.

In addition to the neutron and the X-ray method, the "active target" ionization chamber (IC) method was developed at Gatchina by employing a D-T target as an IC and using the PSI beam. A value of $\omega_s = 0.58(4)$ was obtained at $\phi = 0.17$ by detecting the ratio of α^{++} to $(\mu\alpha)^+$ [93Cas].

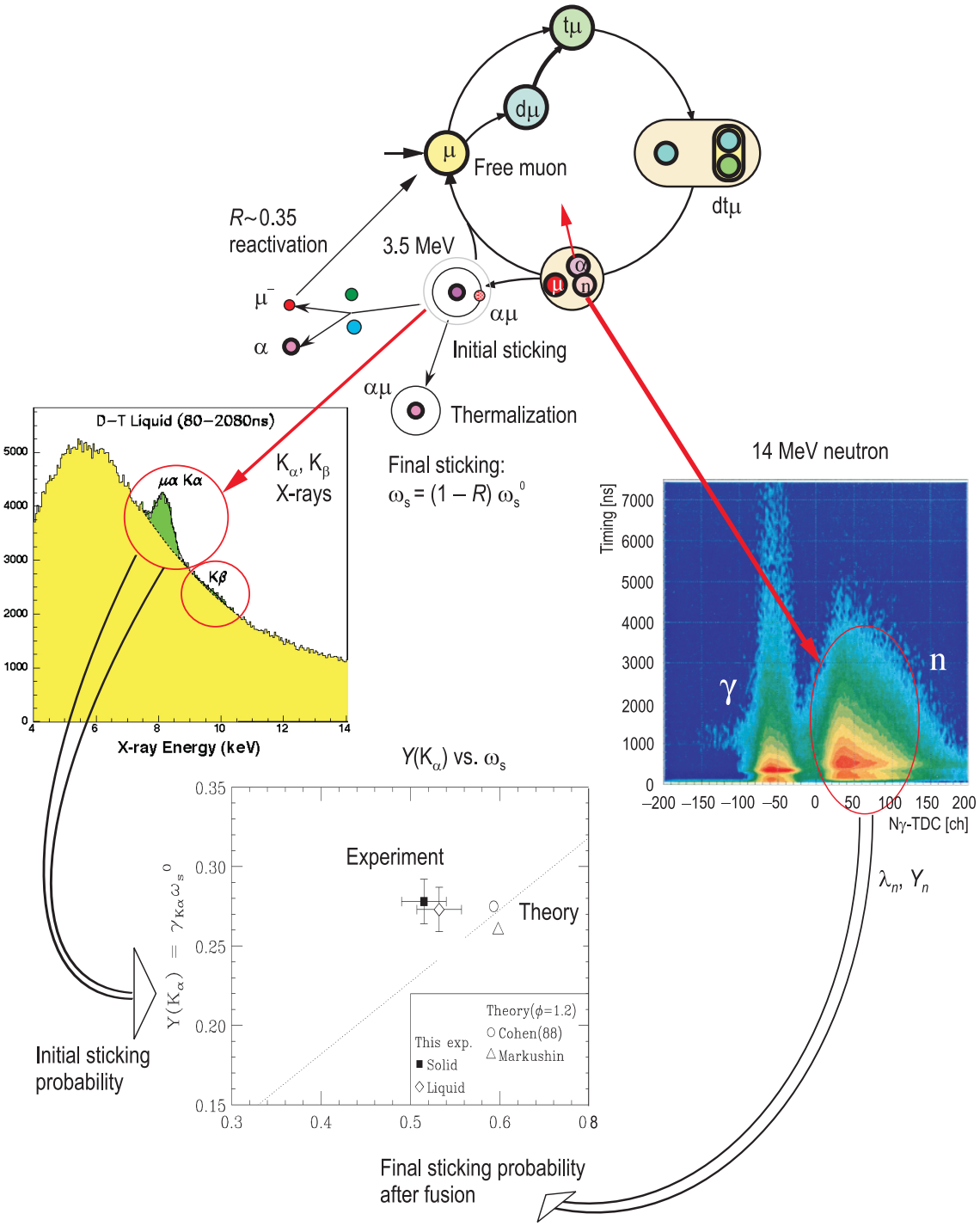

Fig. 11.19. Observed values of the K_α X-ray yield per fusion, $Y(K_\alpha)$, against the effective sticking probability, ω_s, obtained from neutron data for the total loss rate. The measured data are compared with the atomic-process calculations for $\kappa(K_\alpha)$ ($Y(K_\alpha) = \kappa(K_\alpha)\omega_s^0$) and R ($\omega_s = (1–R)\ \omega_s^0$) assuming $\omega_s^0 = 0.912$ % for the initial sticking [88Mar].

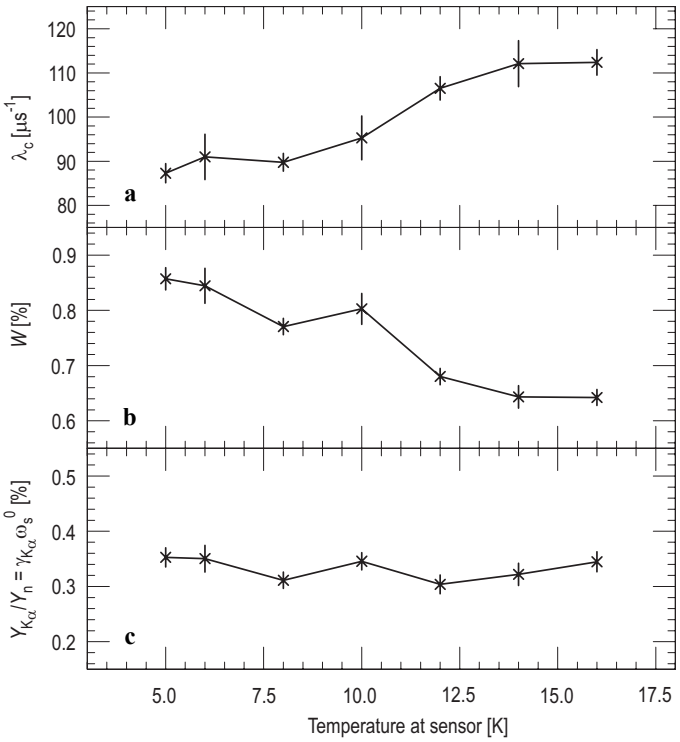

Fig. 11.20. Temperature dependence of **(a)** the muon cycling rate, λ_c, **(b)** the muon-loss probability, W, and **(c)** the ratio of Y_x to Y_n ($Y(K_\alpha)$) in solid D-T with a tritium concentration of 40 % [03Kaw].

11.11 The He impurity effect

The existence of He impurities is an inevitable problem in D-T μCF for the following two reasons: (a) Owing to tritium beta-decay, when there is no ^{3}He removal system, ^{3}He accumulates steadily (100 ppm per day); (b) the amount of ^{4}He produced during D-T μCF also accumulates, which may cause serious problems.

On the other hand, the phenomenon of μ^- transfer from p, d, t to ^{3}He and ^{4}He is of special interest for the following reasons: (a) This transfer reaction is not only known to be the most fundamental process other than transfer among hydrogen isotopes, but also to be anomalously fast compared to the conventional direct-exchange process; (b) this transfer reaction gives us an opportunity to learn about the structure of muon molecules by X-ray spectroscopy.

Historically, the formation of the $(d^4He\mu)$ state was proposed by Popov et al. in order to explain the anomalously high rate of μ^- transfer from hydrogen isotopes to the He impurity [81Ari, 81Kra]. According to this model, the following process is expected to take place (Fig. 11.21): Instead of a direct exchange reaction of $(d\mu) + {}^4He \rightarrow ({}^4He\mu) + d$, the molecular ion is formed through $(d\mu) + {}^4He \rightarrow [(d^4He\mu)\, e^-]^+ + e^-$, where the $(d^4He\mu)$ molecule is preferentially formed in the $J = 1$ state. In this case, the characteristic photon spectrum can be predicted; it features a unique peak energy (6.8 keV versus 8.2 keV of the K_α line in $He\mu$) as well as a broad and asymmetric shape.

At UT-MSL/KEK, such an experiment was carried out for a liquid-D_2 target with He impurity (430 ppm), which was dissolved by pressurizing the liquid-D_2 surface with two atmospheres of He gas [86Mat]. The observed results are shown in Fig. 11.22 for the time-integrated energy spectrum at a delayed time after μ-injection (0.28…7.5 μs). There, a characteristic asymmetric and broad photon peak was observed with a central energy of 6.85(4) keV and a width of 0.74(4) keV, agreeing quite well with the theoretical predictions [81Kra].

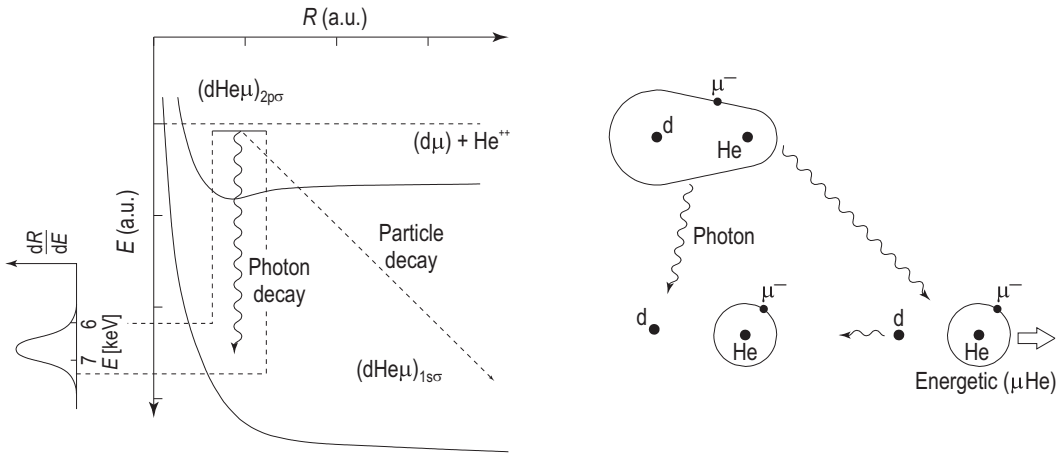

Fig. 11.21. Schematic energy diagram explaining μ^- transfer from d to He through formation of a (dHeμ) molecule including the predicted photon-energy spectrum of the radiative transition.

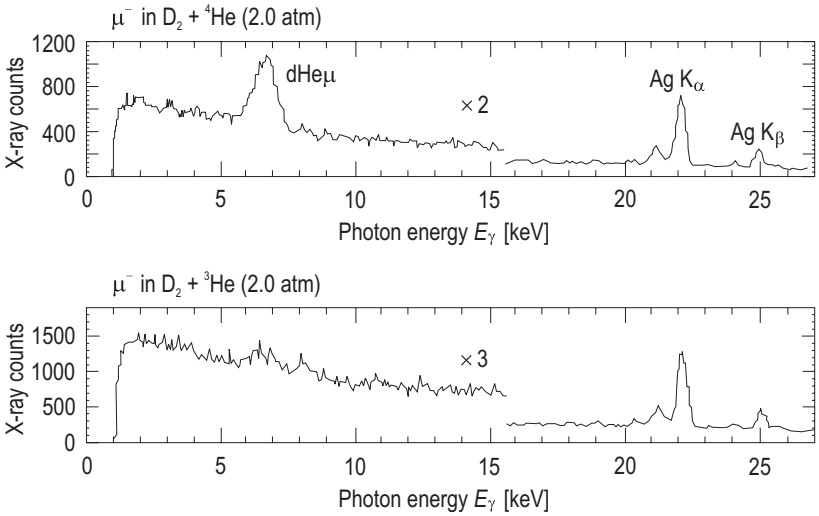

Fig. 11.22. Observed photon spectra from liquid D_2 with 193 ppm of ^{4}He and 250 ppm of ^{3}He, respectively [93Ish].

Based upon the predicted and the observed energy spectra, one can conclude that a radiative-transition photon was observed. The present result nicely confirms the model of muon transfer through the formation of a muon molecule.

After the first X-ray observation of a ($d^4He\mu$) molecule, a (dμ)-to-He transfer experiment was extended to see the isotope effect, namely to study the difference with respect to ^{3}He. The expected nature of the ($d^4He\mu$) molecule in terms of the energies of the molecular levels predicts that no big difference exists between the radiative photon intensities that could be seen in these two transfer reactions.

The X-ray spectra first observed at UT-MSL/KEK [93Ish], as displayed in Fig. 11.22, show a surprising difference at around 6.8 keV; a significant peak can be seen in ($d^4He\mu$), while only a weak one can be seen in ($d^3He\mu$). In combination with the difference in the muon-molecule formation rate and concentration, the ratio between the value of the 6.8 keV photon intensity for ($d^3He\mu$) and that for ($d^4He\mu$) becomes 0.138. Later, similar results and a more precise energy spectrum were obtained at PSI using a CCD detector [96Gar].

There are four decay modes of $(d^{3,4}He\mu)_{J=1}$ which have attracted strong theoretical interest:

1. Radiative decay: $(d^{3,4}He\mu)_{J=1} \rightarrow (^{3,4}He\mu)_{1s} + d + \gamma\,(\approx 6.8\ \text{keV})$,
2. Fusion: $(d^{3}He\mu)_{J=1} \rightarrow {}^{4}He + p + \mu$,
3. Predissociation: $(d^{3,4}He\mu)_{J=1} \rightarrow (^{3,4}He\mu)_{1s} + d$,
4. Auger decay: $[(d^{3,4}He\mu)_{J=1}\ e^{-}] \rightarrow (d^{3,4}He\mu)_{J=0} + e^{-}$.

Calculations of the radiative decay of $(d^4He\mu)$ by Aristov et al. [81Ari] and by Hara and Ishihara [89Har] have explained the observed photon spectrum, which provided the first direct evidence for the existence of muonic molecules. The radiative decay rate λ_r given by [91Kam] is $1.55 \times 10^{11}\ s^{-1}$ for $(d^3He\mu)_{J=1}$ and $1.69 \times 10^{11}\ s^{-1}$ for $(d^4He\mu)_{J=1}$, respectively.

The fusion-reaction rate, λ_f, of $(d^3He\mu)_{J=1}$ is given in Table 11.12. It can be seen that the fusion process is negligible in comparison with radiative decay from the states with $J = 0$ and $J = 1$. It is then needless to say that no fusion occurs in the $(d^4He\mu)$ molecule. Therefore, it is clear that the fusion branch is not an origin of the observed strong reduction of the radiative decay in $(d^3He\mu)$ compared with $(d^4He\mu)$.

It was first predicted by Kamimura [91Kam] that a strongly reduced radiative-decay branching ratio should be observed in case of $(d^3He\mu)$. For $(d^3He\mu)$, particle decay is much stronger than radiative decay, while this is not the case for $(d^4He\mu)$. The enhancement of the particle decay in $(d^3He\mu)$ compared with that in $d^4He\mu$ essentially comes from the fact that the kinetic energy (zero-point oscillation) in the former is larger than that in the latter, simply owing to the smaller mass of ^3He. Along with this consideration, an even stronger reduction of radiative decay in $(p^4He\mu)$ was predicted.

In order to more accurately calculate the width of such highly excited (≈8 keV) Feshbach-type resonances, Kino and Kamimura [93Kin] developed a direct numerical method to solve the resonant states under the explicit scattering boundary condition for the d-$(He\mu)_{1s}$ channel. The resulting energy and width of the $J = 0$ and $J = 1$ resonances, respectively, are listed in Table 11.12 together with the corresponding results by other authors. We can thus see that the branching ratio of the radiative decay is given by

$$\frac{\lambda_r}{\lambda_r + \lambda_p} = \begin{cases} 0.234 & \text{for } \left(d^3He\right)_{J=1} \\ 0.503 & \text{for } \left(d^4He\right)_{J=1} \end{cases} \qquad (11.35)$$

This predicts that the ratio of the radiative decay strength of $(d^3He\mu)$ to that of $(d^4He\mu)$ is 0.234/0.503 = 0.465 as long as the formation probabilities of the two muonic molecular states are normalized to be the same. This ratio explains well the observed value of 0.38 ± 0.06 [93Ish].

Auger decay of the hydrogen-helium muonic molecules was investigated by Kravtsov et al. They concluded that the Auger rate is independent of the isotopic content of the molecule and amounts to ≈25 % of the radiative rate. Although de-excitation from $J = 1$ to $J = 0$ via an inner Auger effect is energetically not allowed for $(dHe\mu)$ molecules, the possibility of de-excitation via an outer Auger effect was pointed out by Czaplinski et al. [96Cza]. More extensive theoretical and experimental studies of the decay mechanism are expected in order to thoroughly understand these interesting muonic molecules.

As a conclusion of this section, it can be said that the rate of μ^- transfer to a He impurity requires ^3He removal to be taken down to a level of 10 ppm as a prerequisite for fundamental studies of energy production from a high-density D-T mixture. In a series of μCF experiments at RIKEN-RAL it was discovered that ^3He originating from the t^- decay does fully stay in a solid D-T mixture, while it disappears in a liquid D-T mixture [99Kaw].

Table 11.12. Properties of different hydrogen-helium-muon molecules. For the $J = 0$ and $J = 1$ states, respectively, the binding energy, E_B, the radiative decay rate, λ_γ, and the predissociation rate, λ_p, are given.

System	Ref.	$J = 0$			$J = 1$		
		E_B [eV]	λ_γ [10^{11} s^{-1}]	λ_p [10^{11} s^{-1}]	E_B [eV]	λ_γ [10^{11} s^{-1}]	λ_p [10^{11} s^{-1}]
($p^3He\mu$)	[a])	69.0	2.11	47.3	38.1	1.74	31.6
($p^4He\mu$)	[a])	75.4	2.24	35.4	45.4	1.89	24.8
($d^3He\mu$)	[a])	70.6	1.80	3.58	48.2	1.58	2.77
	[b])	70.946	1.75 [e])	4.70	48.419	1.55 [e])	5.06
	[c])	70.9764		5.74	48.42109		5.38
	[d])	69.96		8.0	46.75		7.0
($d^4He\mu$)	[a])	78.7	1.94	1.85	57.6	1.74	1.38
	[b])	77.430		1.60	58.221	1.69 [e])	1.67
	[f])				58.225	1.80	
	[d])	77.96		2.3	56.10		2.4
($t^4He\mu$)	[a])	72.3	1.70	0.79	53.4	1.53	0.66

[a]) A.V. Kravtsov et al. [94Kra].
[b]) Y. Kino and M. Kamimura [93Kin].
[c]) L.N. Bogdanova et al. [99Bog].
[d]) S.S. Gerstein and V.V. Gusev [93Ger].
[e]) A. Hara and T. Ishihara [89Har].
[f]) V.I. Korobov [96Kor].

11.12 Applications of μCF

Possible applications of μCF phenomena in various fields have been considered. Here, the following three subjects are discussed: (a) a μCF energy source, (b) a 14 MeV neutron source, and (c) an ultra-slow μ^- source.

11.12.1 A practical energy source using μCF

Before considering the energy-production efficiency, in particular regarding the possibility of break-even achievement, we must emphasize the important features of μCF with regard to the energy problem. As commonly mentioned for fusion energy in general, μCF is a "clean" energy source with a "minimum" production of radioactive waste. Contrary to thermo-nuclear fusion, because of employing the "heavy-electron" nature of the μ^-, there is no need to use very high temperatures; μCF is in fact "cold" fusion. Muon-catalyzed fusion is initiated by an accelerator-produced μ^-, and it can be stopped at the instance of terminating the accelerator operation. Thus, it is a "controlled" atomic energy source.

In order to consider the energy-production efficiency, it is required to know how much energy is needed to produce a single muon (the muon cost). There have been several discussions on the optimization of the π^- production and the $\pi^- \rightarrow \mu^-$ conversion processes. In case of π^- production, the fundamental reactions in the nucleon-nucleon inelastic process are $n + n \rightarrow p + n + \pi^-$ and $n + p \rightarrow p + p + \pi^-$. The cross section of the first process is three times larger than that of the second. For efficient π^- production, the use of accelerated nuclei which contain "accelerated" neutrons is thus inevitable. Energy (cost) estimates towards economic μ^- production have been carried out for deuteron and triton beams.

Following the argument made by Petrov et al. [79Pet], a realistic solution seems to be as follows. Using a 1 GeV/nucleon t (d) beam to bombard Li or Be nuclei, we can obtain 0.22 (0.17) π^- from every t (d). By using a large-scale superconducting solenoid with a reflecting mirror, one can expect 75 % efficiency for μ^- production from a single π^-. Since π^- production is proportional to the incident t (d) beam energy, and a 1 GeV deuteron produces 0.17 μ^-, one μ^- per d (t) can be produced using an energy of 6 (8) GeV. Selecting the corresponding values for π^- production in a t-t collision, the cheapest cost might eventually be about 1 π^-/4 GeV and 1 μ^-/5 GeV.

Several ideas have been proposed for the reduction of the muon cost. Studies have been carried out to optimize the type of particle, the particle energy and the choice of the fixed target, as compiled in Table 11.13. To summarize these studies, optimization does not seem to yield an improvement of the value mentioned above (1 π^-/4 GeV). One possible method to reduce the π^- production cost is to use colliding beams. In this case, the energy of the center-of-mass motion which is wasted in case of a fixed-target geometry would be used efficiently. It is claimed that a production efficiency of 1 π^-/1.8 GeV (0.55 π^-/GeV) could be achieved using a d-d collider. However, the feasibility of such a collider with a power exceeding MW is totally uncertain.

Table 11.13. Examples of pion and muon cost estimates.

Author	Reaction	π^-/E [1/GeV]	μ^-/E [1/GeV]	Condition
Petrov and Shabelski [79Pet, 85Pet1, 85Pet2]	t(1 GeV)-t	0.25	0.20	50 % elastically scattered t is unused
	t(1 GeV)-C, Be	0.22	0.17	
	D(1 GeV)-C	0.17	0.125	
Jändel [88Jae]	d-[D-T($\phi < 0.1$)]		0.5	infinite D-T target
Kuzminov, Petrov and Shabelski [93Kuz]	d(0.9 GeV)-[D-T($\phi = 0.50$)]	0.19		multiple NN collision
Anissinov et al. [01Ani]	d(2 GeV)-C, Be	0.22		internuclear cascade code

On the other hand, the energy-production capability $E_{\mu CF}^{out}$ per single μ^- of the D-T μCF process is determined by $E_{\mu CF}^{out} = 17.6 \times Y_n$ (MeV), for which the sticking probability ω_s constitutes a stringent limiting factor. This can be expressed as $E_{\mu CF}^{out} \leq 17.6\ \omega_s^{-1}$ (MeV). The situation in relation to $E_{\mu CF}^{out}$ is summarized in Fig. 11.23. The scientific break-even point can be achieved for $E_{\mu CF}^{out} > 5$ GeV. As described in Sect. 11.10, based upon recent results at RIKEN-RAL, the most promising way to achieve the break-even point seems to be D-T μCF in a high-temperature condensed phase where an enhanced value of R ($\rightarrow 0.7$) might be obtained.

Several remarks can be made on possibilities of a further increase in the energy-production capability of D-T μCF towards the economic break-even point: (a) Since neither the experimental conditions of the D-T target (such as density ϕ, temperature T and tritium concentration C_t) nor the energy $E_{t\mu}$ of the (tμ) atoms have been satisfactory so far, there might exist more favorable conditions for enhanced energy production; (b) in order to increase $\lambda_{dt\mu}$, a more favorable matching condition in terms of resonant molecular formation may exist which might be accessed by exciting the molecular levels of D_2 or DT using e.g. lasers; (c) in order to decrease ω_s or to increase R, several ideas have been proposed. Among them the use of a D-T plasma (where enhanced regeneration is expected due to an elongated $(\alpha\mu)^+$ mean free path) [89Men] and acceleration of $(\mu\alpha)^+$ using an electric field [90Dan] are two that may be worth trying; (d) owing to collisions between the $(\alpha\mu)^+$ ions and α^{++} ions from nearby μCF reactions, exotic regeneration reactions may occur in high-density D-T mixtures using an intense pulsed μ^- beam: $(\mu\alpha)^+(I) + \alpha^{++}(II) \rightarrow \mu^- + \alpha^{++}(I) + (\alpha)^{++}(II)$.

Table 11.14. Proposed high-intensity μ^- sources at various hadron accelerators.

Project	Institute	Accelerator	p, d/s	μ^-/s	μ^-/p, d	μ^-/MW
L.F.N.C. [a)][b)]	INR-Moscow	p, 500 MeV, 100 μA	6.2×10^{14}	10^{11}	1.6×10^{-4}	2×10^{12}
L.F.N.C. [a)][c)]	AGS-BNL	p, 24 GeV, 3 μA	1.9×10^{13}	4×10^{11}	0.021	5.6×10^{14}
$\mu^+\mu^-$ collider [d)]	BNL etc.	p, 30 GeV, 0.25 μA	$2.3 \times 10^{13}/15$	$4 \times 10^{12}/15$	0.17	3.6×10^{13}
μCF n-nource [e)]	PSI	d, 1.5 GeV, 12 mA	7.5×10^{16}	10^{15}	0.013	5.6×10^{13}
General purpose [f)]	JHF-KEK	p, 3 GeV, 200 μA	1.3×10^{15}	1.3×10^{13}	0.01	2.2×10^{13}
μCF reactor [g)]	Gatchina	d, 1.5 GeV, 12 A	7.5×10^{16}	1.5×10^{16}	0.20	8.0×10^{14}

[a)] Search for lepton-flavor non-conservation.
[b)] [92Aba], [c)] [96Mol], [d)] [96Pal], [e)] [93Pet1, 93Pet2], [f)] [96Nag1, 96Nag2], [g)] [85Pet1, 85Pet2].

In the experiment at RIKEN-RAL, the level of energy production is 3 μW, with $(6\ldots7) \times 10^3$ μ^-/s produced by the superconducting muon channel installed at a 800 MeV × 200 μA proton beam. A 5 mm carbon target is used, and stopping of the μ^- is accomplished in a 1.5 cm^3 liquid/solid D-T target, producing 10^6 fusions/s. The basic ideas of a μCF energy source will make further progress as a result of the development of the high-intensity hadron accelerator and the advanced muon-producing beam channel. In the near future, new accelerator projects like a neutron spallation-source, a neutrino factory and muon colliders may contribute significantly to such progress. Even with the presently available value of the fusion yield of 150 per one μ^-, by employing advanced methods concerning the accelerator or muon production, one could realize a μCF reactor at the kW level. An overview is given in Fig. 11.24.

Considering a number of new trends with regard to μCF processes one might expect a contribution to the development of fusion energy. The distinguished examples are: (1) development of materials for the first wall of the fusion reactor by using a high flux of 14 MeV neutrons from μCF as described below; (2) a tritium-production test facility, where, by employing high spatial fusion-density, the tritium-breeding process at the blanket proposed for a fusion reactor can be examined more easily; (3) a contribution to the studies of plasma instability due to alpha heating, with an application of the μCF process just beside the plasma facility.

As opposed to the production of energy solely via μCF, the concept of a muon-catalyzed hybrid reactor was proposed by Petrov [80Pet] and later by Eliezer et al. [86Eli]. In this concept, the accelerated 1 GeV/nucleon deuteron beam is used to bombard a Li or Be target, with the remainder of the beam stopping in ^{238}U. In this way ≈ 30 % of the beam is spent on π^- production, while 70 % is spent on ^{238}U fission and ^{238}Pu production via electronuclear breeding. The π^- thus produced is used for μCF in a D-T mixture, and the 14 MeV neutron produced in the μCF reaction stops in the blanket of ^{238}U and ^{6}Li yielding ^{239}Pu and T. The Pu fuels a thermal nuclear reactor, and the fission energy is used to feed the accelerator and the rest of the system. The proposers conclude that the hybrid system can double the electric power output of the non-hybrid electronuclear breeding. However, it must be noted that the use of μCF for fuel production in a thermal nuclear reactor is accompanied with all the usual problems of nuclear reactors such as radioactive waste disposal, etc.

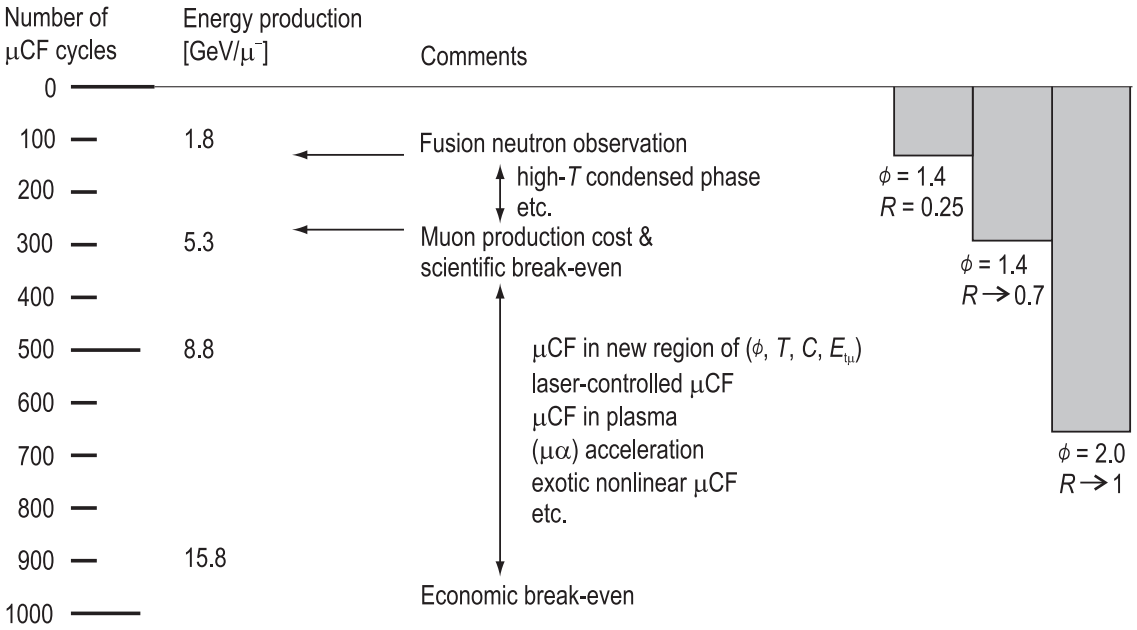

Fig. 11.23. Number of fusion reactions and amount of energy produced in D-T μCF, as well as the expected future increase under the assumed changes in density (ϕ) and regeneration factor (R).

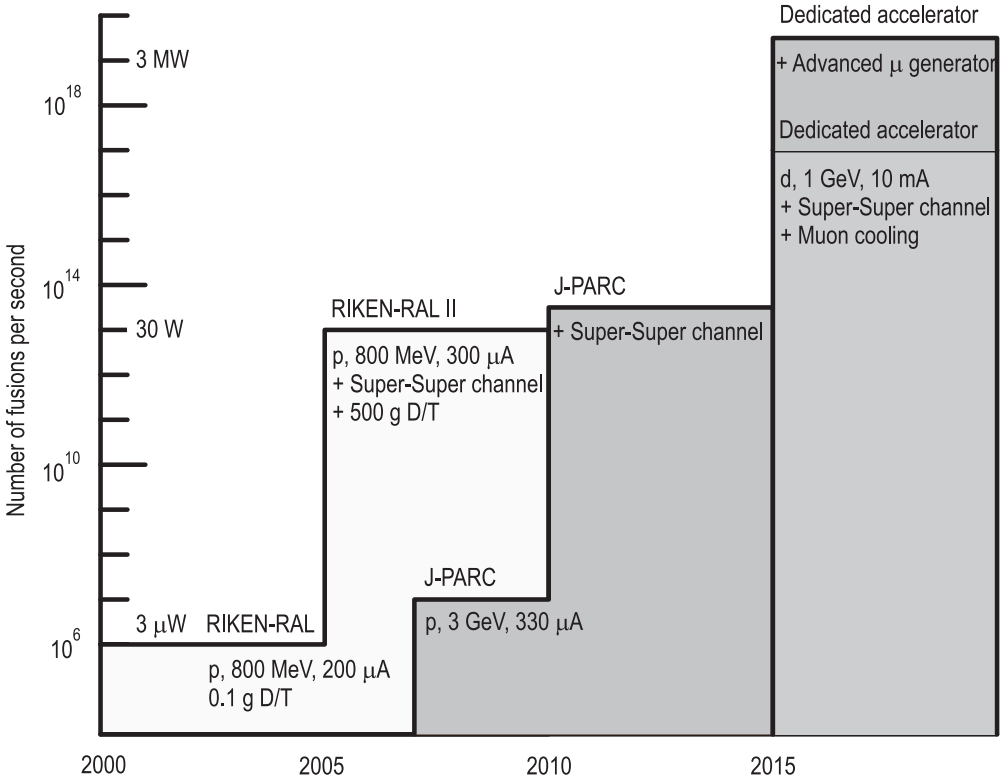

Fig. 11.24. Expected increase in the power generation of D-T μCF against expected progress of the accelerator power as well as of the method of muon-beam production. Here a fusion rate of 150/μ^- is assumed.

11.12.2 A 14 MeV neutron source using μCF

When thermal nuclear fusion becomes feasible, it is important to develop materials to be used for the first wall next to the innermost core of the thermal fusion reactor. For this purpose, it is necessary to have an irradiation-test facility where candidate materials can be tested under a very high flux of 14 MeV neutrons. One practical idea is to have an intense 200 keV deuteron beam as primary beam and produce 14 MeV neutrons via the reaction $d + t \rightarrow \alpha + n$. In parallel to this idea, the 14 MeV neutrons from μCF can be considered an alternative for such a material-irradiation facility.

Some promising schemes have been considered [93Pet1, 01Ani]. Let us assume that a 2 GeV × 12 mA deuteron accelerator becomes available. By placing a 150 cm long lithium target of 0.75 cm radius under the confining field of a 17/7 T superconducting solenoid, intense pion production and efficient μ^- production can be realized. In this scenario, μCF occurring in a D-T target into which the intense μ^- beam is directed produces an intense flux of 14 MeV neutrons of the order of 10^{14} $cm^{-2}s^{-1}$ in a test volume of ≈ 2.5 ℓ with a surface of ≈ 350 cm^2. The material to be tested is placed on one surface of the D-T container. Most importantly, the power consumption by the μCF method is substantially lower than by the deuteron-accelerator method. Some realistic plant-design work is now in progress.

11.12.3 Slow-μ^- generation via μCF

For the case of negative muons (μ^-), it has been found to be very difficult to produce an intense beam of slow μ^- because of the following reasons: (1) Owing to a strong absorption of stopped π^- inside matter, the π^--to-μ^- decay cannot be realized inside the target material, so that, contrary to μ^+, there is no surface μ^-, except for a small probability for liquid H_2 or He; (2) because of muonic-atom formation, the stopped μ^- cannot be liberated from the stopping material after thermalization inside condensed matter, and thus no re-emission can be expected for μ^-. The situation is of course very different for slow-μ^+ production.

In order to overcome the second difficulty, a new idea has been proposed for a source of slow μ^-, which will be realized with the help of μCF phenomena [89Nag]. The principle is as follows: (a) At the disappearance of the core nuclei of ^{5}He at the instant of μCF, a slow μ^- with an energy of around 10 keV is released; (b) this liberation process is known to be repeated up to 150 times during the μ^- lifetime; (c) after a number of successive liberation processes of slow μ^-, we can expect that a significant fraction of the μ^- stopping inside a thin, solid D-T layer would be re-emitted from the surface.

When there are no leakage processes from the D-T layer (solid and $C_t \approx 0.3 \ldots 0.5$), the conversion efficiency can be estimated to be the ratio of the range of the 10 keV μ^- (0.3 μm) to that of the incoming μ^- with an energy of, say, 1 MeV (0.9 mm). The multiplication factor due to the number of μCF cycles is $\approx \sqrt{150}$, thus giving $\sqrt{150} \times 0.3 \times 10^{-3} / 0.9 = 0.004$. For a more realistic estimate, the kinetics in μCF must be taken into account. For instance, the diffusion length of the neutral (dμ) or (tμ) gives a significant correction to the value mentioned above. Assuming 1 μm for the diffusion length of (dμ) and (tμ) in the D-T layer with a thickness of 7 μm, the conversion efficiency for stopping a 1 MeV μ^- to the slow μ^- (below 10 keV) emission is around 2×10^{-4} instead of 4×10^{-3}.

In order to enhance the conversion efficiency, a two-layer structure was proposed by G.M. Marshall featuring an optimized D-T layer on a 1 mm thick H_2 layer with 0.1 % T_2. The range of the injected MeV μ^- can effectively be reduced by the Ramsauer-Townsend effect.

The generation of intense, slow μ^- has an important field of application, namely as a μ^- ion source for $\mu^+\mu^-$ colliders. A circular lepton collider in the TeV range is possible only with muons as they feature much lower energy loss through synchrotron radiation than electrons and yet live long enough to form colliding beams. A slow-muon source, as already realized for μ^+ [95Nag, 94Mor], along with the slow-μ^- source described here, can efficiently be used for a realistic method of muon cooling [96Nag1, 96Nag2]. The μ^- cooling in turn may open a new development of μCF, in particular to realize very high fusion-density phenomena.

11.12.4 Power generation at the kW level before 2010

In order to gain public understanding of fusion energy, it is interesting and important to demonstrate the stable and long-term operation of fusion-generated power at the kW level in a fully controlled manner as soon as possible, hopefully before 2010. For this purpose, a promising candidate is the μCF power generator to be installed at the proposed 5 MW proton accelerator. A realistic scheme is proposed in Table 11.15 and Fig. 11.25, where the μCF power generator works in parasitic mode, i.e. with the major use of the intense proton beam, like a neutron spallation-source, located downstream. A value of 150 μCF/μ^- is assumed.

Table 11.15. Parameters for realization of μCF power generation at the kW level.

	$(SUPER)^2$ at ISIS-II, K. Ishida et al. [98Ish]	kW μCF reactor
$I_P \times E_p$	60 μA × 800 MeV	5 mA × 1 GeV
Target	4 cm, C	4 cm, C
Total π^- production	1.2×10^{12}/s	1.2×10^{14}/s
Gain factor	≈ 100	≈ 100
$\pi^- \rightarrow \mu^-$	0.025	0.025 $(1 + \alpha)$ [a]
μ^- stopping in D-T	$3 \times 10^{10}\ \varepsilon_1$	$3 \times 10^{12} \times (1 + \alpha)(1 + \beta)\ \varepsilon_1$ [b]

[a]) α: solenoid reflection at the upstream end, $\alpha \approx 0.10$ (μCF Intense Neutron Source [01Ani]).
[b]) β: solenoid reflection at the downstream end, need $1 + \alpha + \beta > \varepsilon_1^{-1}$.

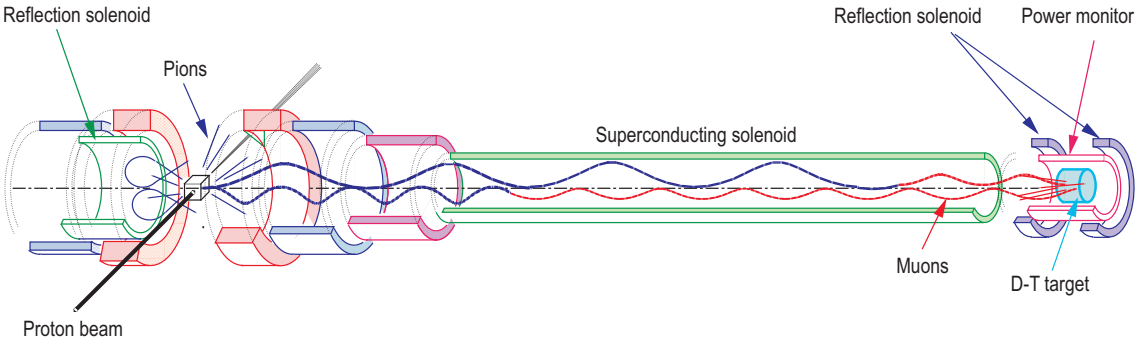

Fig. 11.25. Schematic layout of the kW μCF power generator to be installed parasitically at the high-intensity proton accelerator.

11.13 Conclusions and future perspectives

The present understanding of muon-catalyzed fusion and the future perspectives towards fusion energy are summarized below. These considerations are again confined to D-T μCF.

(1) Some important experimental facts of D-T μCF are still lacking explanation, in particular concerning μCF in a high-density, condensed-matter phase of the D-T mixture. A distinguished example is the rate of muon-molecule formation, $\lambda_{dt\mu}$, in liquid and solid D-T mixtures, for which theory predicts a reduced value while experiments have shown it to be particularly high. Moreover, in liquid and solid D-T mixtures an anomalously large regeneration factor exists for the $(\alpha\mu)^+$ formed during the fusion process in the $(dt\mu)$ molecule.

(2) A realization of the scientific break-even point of 300 fusions per single μ^- seems to be possible in the near future. The presently realized numbers of 150 fusions/μ^-, effective sticking probability $\omega_s = 0.44$ % and regeneration factor $R = 0.52$ can be replaced by numbers such as 300 fusions/μ^-, $\omega_s = 0.33$ % and $R = 0.70$ by at least two schemes: (a) Extrapolating the anomalous temperature dependence of R, one can expect enhanced R in pressurized and high-temperature (above 20 K), solid D-T; (b) by introducing high-intensity, pulsed μ^-, one can expect a nonlinear, exotic, μCF-like, correlated fusion phenomenon to enhance R.

(3) If a large-scale μCF setup is realized, it may contribute to fusion-energy research and development. By employing high-intensity muon generation, one can realize fusion phenomena with extremely high spatial density. Thus, a μCF plant can be used for e.g. (a) an intense 14 MeV neutron source for the development of wall materials of a fusion reactor, and (b) tritium fuel production.

(4) The realization of a μCF reactor at the kW level at an intense hadron accelerator in the near future is urgently required to demonstrate the feasibility of fusion energy to the public.

11.14 Concluding remarks on a possible μCF power plant

Optimistically seen, the future development of μCF can lead to a real power plant. The accelerator employed is considered to be used exclusively for μCF power generation, although it could also be used to produce additional energy as a by-product, as described in the final part of Sect. 11.12.1.

A dedicated μCF power plant can only be realized after the economic break-even point has been achieved. Here we take the following assumptions for an enhanced energy-production capability based upon a favorable extension of the presently available experimental facts:

(1) Realization of $R \rightarrow 1$ in a high-T, condensed phase of $\phi = 2.0$, as suggested by the recent RIKEN-RAL data [03Kaw].

(2) Continuation of the relation $\lambda_c \propto \phi$ up to $\phi = 3.0$ in a high-T, condensed phase, as expected from Fig. 11.16.

Then one can expect values λ_c of 200×10^6 s^{-1} and Y_n ($= \phi\lambda_c/\lambda_0$) of 1320/$\mu^-$.

The advanced, superconducting deuteron linac at the 10 MW (1 GeV × 10 mA) level which requires 15 MW of electric-power input will be constructed for the exclusive use of μCF power generation. One can expect 0.20 π^-/d by colliding accelerated d with a C or Be target [01Ani], and 0.15 μ^-/d by a $\pi \rightarrow \mu$ converter [79Pet, 01Ani]. Thus, the generation of power by μCF will yield

$$0.15 \times 10\ \text{mA} \times 17.6\ \text{MeV} \times 1320 \rightarrow 35\ \text{MW} \tag{11.36}$$

which can be converted to 15 MW electric-power output to cover the electric power of the linac.

A further increase in the energy produced can be expected by a higher value of λ_c which is realized by increasing $\lambda_{dt\mu}$. One possibility to achieve this goal is by the contribution of a high-energy resonance at high ϕ and high temperature. This should be investigated by the future experiments.

Acknowledgements

The author acknowledges the contributions of his collaborators in the μCF studies: Drs. T. Matsuzaki, K. Ishida, S.N. Nakamura, N. Kawamura, A. Toyoda, M. Tanase, M. Kato, H. Sugai, G.H. Easton, T. Koike, Y. Kino and Professor M. Kamimura. Helpful discussions with Professors L.I. Ponomarev, M. Faifman, L. Bogdanova, S.E. Jones and Drs. M. Leon, J.S. Cohen, G.M. Marshall and C. Petitjean are also acknowledged. The author is grateful to encouragements from Professor T. Yamazaki, T. Nishikawa, H. Sugawara, A. Arima, S. Kobayashi, the late M. Oda and P.W. Williams.

11.15 Appendix

11.15.1 Numerical data on D-T μCF

11.15.1.1 (dtμ) formation rate

(1) Data on the cycling rate λ_c for gaseous and liquid/solid D-T at PSI [99Ack].
$13.0\ \mathrm{K} < T < 41.4\ \mathrm{K}$, $0.032 < \phi < 1.45$, $0.028 < C_t < 0.42$.

Data point	ϕ	eq/ neq	T [K]	λ_c [μs^{-1}]	Error [μs^{-1}]
$C_t = (41.8 \pm 1.4)$ %					
1.	1.20	neq [a])	22.5	130.01	2.63
2.	1.45	eq	13.0	111.32	2.29
3.	1.19	eq	23.0	110.00	2.63
4.	0.975	eq	33.3	100.00	2.19
5.	0.25	eq	41.4	79.86	3.28
6.	0.125	eq	42.6	71.76	4.18
7.	0.032	eq	30.9	57.41	3.52
$C_t = (88.4 \pm 1.0)$ %					
8.	1.19	neq [b])	25.3	27.68	3.09
9.	1.50	eq	13.5	6.214	2.80
10.	1.21	eq	24.4	5.889	3.18
11.	0.238	eq	41.2	4.207	4.47
12.	0.106	eq	39.9	3.464	6.08
$C_t = (21.0 \pm 0.8)$ %					
13.	1.190	eq	22.1	79.82	2.60
14.	0.118	eq	37.0	66.25	3.44
$C_t = (61.7 \pm 1.7)$ %					
15.	1.180	eq	24.7	72.15	2.67
16.	0.122	eq	37.7	38.34	3.38
$C_t = (2.85 \pm 0.4)$ %					
17.	1.160	eq	23.3	9.647	2.63
18.	1.117	eq	36.8	10.26	3.91

[a]) Concentration of D_2: 38.9 ± 3.5 %.
[b]) Concentration of D_2: 4.9 ± 2.5 %.

(2) Data on the cycling rate λ_c for gaseous and liquid/solid D-T at RIKEN-RAL [03Kaw].
16 K < T < 20 K, 1.22 < ϕ < 1.47, 0.10 < C_t < 0.70.

C_t	ϕ	λ_c [μs^{-1}]	Error [μs^{-1}]
10 %	1.2245	32.4	0.8
	1.4168	39.7	1.0
20 %	1.2327	69.9	1.7
	1.4270	76.3	2.0
30 %	1.2376	89.4	2.2
	1.4327	101.6	3.0
40 %	1.2449	110.6	2.7
	1.4419	115.0	4.0
50 %	1.2516	101.2	1.3
	1.4519	102.6	1.8
60 %	1.2580	79.2	1.9
	1.4602	84.6	2.3
70 %	1.2650	53.2	1.3
	1.4680	57.8	1.8

11.15.1.2 Muon loss rate and X-rays from sticking

(1) Data on the loss rate W, the effective sticking probability ω_s and the K_α X-ray yield (photon/fusion) from μ-α sticking in liquid/solid D-T at RIKEN-RAL [03Ish].

C_t	W [%]	Error [%]	ω_s [%]	Error [%]	$Y(K_\alpha)$ [%]	Error [%]
(liquid)						
0.1071	0.811	0.027	0.650	0.027	0.282	0.013
0.2098	0.646	0.015	0.553	0.015	0.287	0.010
0.3035	0.635	0.014	0.560	0.014	0.260	0.006
0.4101	0.642	0.009	0.560	0.009	0.277	0.008
0.5171	0.628	0.009	0.513	0.009	0.310	0.012
0.6201	0.642	0.015	0.455	0.015	0.255	0.015
0.7140	0.793	0.019	0.466	0.019	0.238	0.018
(solid)						
0.1022	0.696	0.028	0.552	0.028	0.312	0.013
0.2021	0.607	0.017	0.527	0.017	0.267	0.009
0.2961	0.577	0.017	0.509	0.017	0.276	0.012
0.4033	0.612	0.014	0.530	0.014	0.286	0.012
0.5026	0.625	0.017	0.506	0.017	0.286	0.015
0.6028	0.679	0.023	0.485	0.023	0.254	0.015
0.7012	0.808	0.032	0.458	0.032	0.275	0.021

(2) Data on the effective sticking probability ω_s, the K_α yield (photon/fusion) and the K_α/K_β yield ratio of X-rays from μ-α sticking in liquid/solid D-T at RIKEN-RAL [02Ish] including data from LAMPF and PSI.

	ω_s [%]	$Y(K_\alpha)$ [%]	$Y(K_\beta)/Y(K_\alpha)$
Theory			
Cohen [88Str1, 88Str2]	0.58 ± 0.005	0.25	0.12
Markushin [88Mar]	0.58	0.25	0.12
Experiment			
LAMPF [93Jon]	0.43 ± 0.05 ± 0.006		
PSI [87Bre]		0.45 ± 0.05	
PSI [a]) [93Pet2]		0.48 ± 0.02 ± 0.04	
PSI [b]) [01Pet]		0.53 ± 0.04	
PSI [87Bos]		0.019 ± 0.05 (C_t = 0.0004)	≤ 0.08
RIKEN-RAL [02Ish] (liquid)	0.532 ± 0.030	0.273 ± 0.017 (C_t = 0.1…0.7)	0.075 ± 0.010
RIKEN-RAL [02Ish] (solid)	0.515 ± 0.030	0.279 ± 0.017 (C_t = 0.1…0.7)	0.060 ± 0.012

[a]) Time-slope method.

[b]) Ionization-chamber method.

(3) Data on the cycling rate λ_c, the loss rate W, the effective sticking probability ω_s and the K_α yield of X-rays from μ-α sticking, normalized by the fusion neutron yield $Y(K_\alpha)$, in liquid/solid D-T at RIKEN-RAL [03Kaw].
5.0 K < T < 16 K.

T [K]	λ_c [μs^{-1}]	Error [μs^{-1}]	W [%]	Error [%]	Y_x/Y_n [%]	Error [%]
5	87.2971	2.17325	0.857217	0.0199928	0.35271	0.017299
6	90.9848	5.14502	0.8444	0.0316077	0.350379	0.0240208
8	89.7722	2.01234	0.770669	0.0149012	0.311264	0.0148267
10	95.3075	4.95654	0.802831	0.0279138	0.345628	0.0157197
12	106.526	2.65209	0.68027	0.0148845	0.304	0.01696
14	112.114	5.203	0.6433	0.0203	0.322	0.02
16	112.391	2.91088	0.64226	0.014485	0.344604	0.0180204

(4) Data on the cycling rate λ_c (normalized to $\phi = 1$), the effective muon loss rate W and the fusion neutron yield Y_n at Dubna [01Bom]. Experimental errors are stated in brackets.

$T = 300$ K

ϕ [LHD]	C_t [%]	λ_c [μs^{-1}]	W [%]	Y_n [neutrons/μ^-]
0.300 (0.012)	17.9 (0.2)	69.8 (3.5)	2.2 (0.2)	23.4 (1.2)
0.295 (0.012)	36.1 (0.3)	101.8 (5.1)	1.1 (0.1)	40.3 (2.0)
0.310 (0.012)	52.0 (0.5)	77.2 (3.9)	1.3 (0.1)	33.1 (1.6)
0.310 (0.012)	68.8 (0.5)	48.2 (2.4)	1.4 (0.1)	23.9 (1.2)
0.434 (0.016)	15.4 (0.5)	57.9 (2.9)	0.91 (0.09)	39.0 (1.9)
0.425 (0.016)	32.7 (1.0)	101.6 (5.1)	0.88 (0.09)	54.1 (2.7)
0.409 (0.016)	47.7 (1.0)	90.1 (4.5)	0.91 (0.09)	48.4 (2.4)
0.411 (0.016)	68.5 (0.5)	50.5 (2.6)	1.2 (0.1)	30.3 (1.5)
0.515 (0.021)	18.2 (0.2)	73.1 (3.7)	2.0 (0.2)	32.2 (1.6)
0.518 (0.021)	35.2 (0.3)	106.2 (5.3)	1.3 (0.1)	48.6 (2.4)
0.532 (0.021)	52.8 (0.5)	89.6 (4.5)	1.0 (0.1)	54.5 (2.7)

$T = 550$ K

ϕ [LHD]	C_t [%]	λ_c [μs^{-1}]	W [%]	Y_n [neutrons/μ^-]
0.289 (0.012)	17.9 (0.2)	80.3 (4.0)	1.9 (0.2)	25.3 (1.2)
0.280 (0.012)	36.1 (0.3)	137.2 (6.9)	1.1 (0.1)	46.3 (2.3)
0.283 (0.012)	52.0 (0.5)	142.8 (7.2)	1.1 (0.1)	45.8 (2.3)
0.289 (0.012)	68.8 (0.5)	105.2 (5.3)	1.0 (0.1)	41.7 (2.1)
0.407 (0.016)	15.4 (0.5)	66.8 (3.3)	0.85 (0.09)	40.4 (2.0)
0.399 (0.016)	32.7 (1.0)	128.8 (6.5)	0.94 (0.09)	59.5 (3.0)
0.383 (0.016)	47.7 (1.0)	135.2 (6.8)	0.84 (0.08)	61.3 (3.0)
0.385 (0.016)	68.5 (0.5)	103.5 (5.2)	1.0 (0.1)	50.1 (2.5)
0.505 (0.021)	18.2 (0.2)	78.5 (3.9)	1.8 (0.2)	34.4 (1.7)
0.490 (0.021)	35.2 (0.3)	128.1 (6.4)	1.2 (0.1)	53.5 (2.7)
0.502 (0.021)	52.8 (0.5)	133.9 (6.7)	0.85 (0.09)	70.7 (3.5)

$T = 800$ K

ϕ [LHD]	C_t [%]	λ_c [μs^{-1}]	W [%]	Y_n [neutrons/μ^-]
0.273 (0.012)	17.9 (0.2)	78.8 (3.9)	2.1 (0.2)	24.5 (1.2)
0.268 (0.012)	36.1 (0.3)	156.0 (7.8)	1.2 (0.1)	42.5 (2.1)
0.273 (0.012)	52.0 (0.5)	169.0 (8.5)	1.1 (0.1)	49.4 (2.4)
0.273 (0.012)	68.8 (0.5)	142.2 (7.1)	1.2 (0.1)	42.5 (2.1)
0.400 (0.016)	15.4 (0.5)	86.5 (4.4)	1.9 (0.2)	31.7 (1.6)
0.375 (0.016)	32.7 (1.0)	154.9 (7.8)	1.4 (0.1)	47.7 (2.4)
0.397 (0.016)	47.7 (1.0)	162.9 (8.2)	1.1 (0.1)	57.1 (2.8)
0.368 (0.016)	68.5 (0.5)	142.5 (7.2)	1.3 (0.1)	47.8 (2.4)
0.484 (0.021)	18.2 (0.2)	70.0 (3.5)	1.8 (0.2)	35.6 (1.8)
0.484 (0.021)	35.2 (0.3)	139.8 (7.0)	1.3 (0.1)	52.4 (2.6)
0.491 (0.021)	52.8 (0.5)	156.9 (7.9)	1.1 (0.1)	61.2 (3.0)

11.15.2 Numerical data on D_2 μCF

11.15.2.1 (ddμ) formation rate and hyperfine transition rate λ_{hf}

(1) Data on the formation rates $\lambda_{1/2}$ and $\lambda_{3/2}$ (normalized to $\phi = 1$) as well as on the hf transition rate $\lambda_{3/2\to1/2}$ in gaseous D_2 at PSI [99Pet1, 99Pet2].

T [K]	ϕ [%]	$\lambda_{1/2}$ [$10^6\,s^{-1}$]	$\lambda_{3/2}$ [$10^6\,s^{-1}$]	$\lambda_{3/2\to1/2}$ [$10^6\,s^{-1}$]
28.3	2.76	0.049(3)	4.04(5)	36.8(4)
32.2	5.14	0.0500(10)	4.20(7)	37.0(3)
36.2	5.14	[0.051]	4.07(6)	36.6(2)
40.3	5.135	[0.0515]	4.07(6)	36.3(2)
45.3	5.05	0.0501(8)	3.98(6)	36.8(3)
50.2	5.13	[0.052]	4.06(6)	[36.0]
52.5	5.05	0.0530(7)	3.77(4)	36.1(16)
60.3	5.04	0.0620(10)	3.96(6)	35.94(25)
72.9	5.04	0.0860(10)	3.96(5)	35.36(25)
96.5	5.02	0.236(3)	4.26(7)	34.7(4)
120.3	4.99	0.531(4)	5.09(10)	35.2(5)
150.3	4.97	0.946(5)	5.17(15)	36.0(9)
200.2	4.94	1.639(20)	4.64(15)	34.0(1.5)
250.1	4.89	2.195(27)	4.22(12)	35.1(2.0)
300.0	4.853	2.541(23)	3.72(9)	36.0(4.0)
350.0	4.814	2.70(5)	[3.27]	[36]

(2) Data on the formation rates $\lambda_{1/2}$ and $\lambda_{3/2}$ (normalized to $\phi = 1$) as well as on the hf transition rate $\lambda_{3/2\to1/2}$ in liquid D_2 at PSI [89Nae].

$\lambda_{1/2}$	$[5.00 \pm 0.34\ (stat.) \pm 0.22\ (syst.)] \times 10^4\,s^{-1}$
$\lambda_{3/2}$	$[3.25 \pm 0.23\ (stat.) \pm 0.23\ (syst.)] \times 10^6\,s^{-1}$
$\lambda_{3/2\to1/2}$	$[3.05 \pm 0.04\ (stat.) \pm 0.06\ (syst.)] \times 10^7\,s^{-1}$
$\gamma = \lambda_{3/2}/\lambda_{1/2}$	$65.0 \pm 1.5\ (stat.) \pm 5.1\ (syst.)$

(3) Data on the ratio of the formation rates $\lambda_{3/2}$ to $\lambda_{1/2}$ and on the hf transition rate $\lambda_{3/2\to1/2}$ in solid D_2 at Dubna [96Dem].

T [K]	ϕ [LHD]	$\lambda_{3/2}/\lambda_{1/2}$	$\lambda_{3/2\to1/2}$ [$10^6\,s^{-1}$]
5.5 ± 0.3	1.43 ± 0.04	58.8 ± 1.8	31.2 ± 1.1
9.9 ± 0.2	1.43 ± 0.04	57.0 ± 1.8	30.4 ± 1.1
15.1 ± 0.2	1.42 ± 0.04	58.1 ± 2.4	31.6 ± 1.3
17.7 ± 0.2	1.40 ± 0.04	61.7 ± 1.7	32.2 ± 1.2
19.0 ± 0.2	1.31 ± 0.04	60.1 ± 1.9	29.4 ± 1.1
26.3 ± 0.3	1.19 ± 0.04	77.9 ± 3.2	32.6 ± 1.2
30.5 ± 0.3	1.08 ± 0.04	72.9 ± 2.8	31.4 ± 1.2

11.16 References for 11

37And Anderson, C.D., Neddermeyer, S.H.: Phys. Rev. **51** (1937) 884.
47Fra Frank, F.C.: Nature **160** (1947) 525.
48Sak Sakharov, A.D.: Report FIAN 1 (1948).
57Alv Alvarez, L.W. et al.: Phys. Rev. **105** (1957) 1127.
57Jac Jackson, J.D.: Phys. Rev. **106** (1957) 330.
57Lin Lindernbaum, S.J., Sternhaimer, R.M.: Phys. Rev. **105** (1957) 1874.
58Wes West, O.: Rep. Prog. Phys. **21** (1958) 271.
67Ves Vesman, E.A.: JETP Lett. **5** (1967) 91.
72Wil Williams, R.W., Williams, D.L.: Phys. Rev. **D 6** (1972) 737.
74Eng Engfer, R. et al.: Atomic/Nuclear Data Tables **14** (1974) 509.
75Zav Zavattini, E.: Muon Physics 2, eds. Huges, V.W. and Wu, C.S., Academic Press (1975) 219.
75Phi Phillips, A.C. et al.: Nucl. Phys. **A 237** (1975) 493.
77Ger Gerstein, S.S., Ponomarev, L.I.: Phys. Lett. **B 72** (1977) 80.
77Hue Hüfner, J. et al.: Muon Physics 1, eds. Huges, V.W. and Wu, C.S., Academic Press (1979) 202.
78Bra Bracci, L., Fiorentini, G.: Nuovo Cimento **A 43** (1978) 649.
79Pet Petrov, Yu.V., Sabelski, Yu.M.: Sov. J. Nucl. Phys. **30** (1979) 66.
79Vin Vinitsky, S.I. et al.: Sov. J. Phys. JETP **47** (1979) 444.
80Bor Borie, E., Leon, M.: Phys. Rev. **A 21** (1880) 1460.
80Pet Petrov, Y.V.: Nature **285** (1980) 466.
80Vin Vinitsky, S.I. et al.: Sov. J. Phys. JETP **52** (1980) 353.
81Ari Aristsov, Yu.A. et al.: Sov. J. Nucl. Phys. **22** (1981) 564.
81Bys Bystritsky, V.M. et al.: Sov. Phys. JETP **53** (1981) 877.
81Kra Kravtsov, A.V. et al.: Phys. Lett. **A 83** (1981) 379.
81Nag Nagamine, K.: Hyperfine Interactions **8** (1981) 787.
82Bog Bogdanova, L.N.: Sov. Phys. JETP **56** (1982) 931.
82Vin Vinitsley, S.I. et al.: Sov. Phys. JETP **55** (1982) 578.
83Jon Jones, S.E. et al.: Phys. Rev. Lett. **52** (1983) 1757.
83Kam Kammel, P. et al.: Phys. Rev. **A 28** (1983) 2611.
83Pon Ponomarev, L.I.: Atomkernenerg./Kerntechnik **43** (1983) 3.
84Bal Balin, V.D. et al.: Phys. Lett. **B 141** (1984) 173.
84Bar Bardin, G. et al.: Phys. Lett. **B 137** (1984) 135.
84Gio Giovanetti, K.L. et al.: Phys. Rev. **D 29** (1984) 343.
84Kra Kravtsov, A.V. et al.: JETP Lett. **40** (1984) 857.
85Cep Cerperley, D., Alder, B.J.: Phys. Rev. **A 31** (1985) 1999.
85Goc Gocheva, A.D. et al.: Phys. Lett **B 153** (1985) 349.
85Leo Leon, M., Cohen, J.S.: Phys. Rev. **A 31** (1985) 2680.
85Pet1 Petrov, Yu.V.: Atomkernenerg./Kerntechnik **46** (1985) 25.
85Pet2 Petrov, Yu.V.: Phys. Lett. **B 163** (1985) 28.
86Bel Beltrami, I. et al.: Nucl. Phys. **A 451** (1986) 679.
86Bog Bogdanova, L.N. et al.: Nucl. Phys. **A 454** (1986) 653.
86Cha Chapline, G., Moir, R.: LLNL Report (1986).
86Eli Eliezer, S., Tajima, T., Rosenbluth, M.: Nucl. Phys. **27** (1987) 527.
86Jon Jones, S.E. et al.: Phys. Rev. Lett. **56** (1986), 588.
86Hu Hu, C.-Y.: Phys. Rev. **A 34** (1986) 2536.
86Mat Matsuzaki, T. et al.: Muon Catalyzed Fusion **2** (1986) 217.
86Men Menshikov, L.I., Ponomarev, L.I.: Phys. Lett. **B 167** (1986) 141.
86Vin Vinitsky, S.I. et al.: Sov. Phys. JETP **64** (1986) 417.
87Bos Bossy, H. et al.: Phys. Rev. Lett **59** (1987) 2864.
87Bre Breunlich, W.H. et al.: Muon catalyzed Fusion **1** (1987) 121.

87Coh Cohen, J.S.: Phys. Rev. Lett. **58** (1987) 1407.
87Kam Kamimura, M.: Muon Catalyzed Fusion **1** (1987) 333.
87Kor Korobov, V.I. et al.: Phys. Lett. **B 196** (1987) 272.
87Nag1 Nagamine, K., Matsuzaki, T., Ishida, K. et al.: Muon Catalyzed Fusion **1** (1987) 137.
87Nag2 Nagamine, K. (ed.): Proceedings of μCF-86 (Tokyo); Muon Catalyzed Fusion **1** (1987).
87Sza Szalewicz, K. et al.: Phys. Rev. **A 336** (1987) 5494.
87Tak Takahashi, H.: Muon Catalyzed Fusion **1** (1987) 623.
88Ada Adamczak, A., Melezhik, V.S.: Muon Catalyzed Fusion **2** (1988) 131.
88Ale Alexander, S.A., Monkhorst, H.J.: Phys. Rev. **A 38** (1988) 26.
88Bog Bogdanova, L.N.: Muon Catalyzed Fusion **3** (1988) 359.
88Eat Eaton, G.H. et al.: Nucl. Instr. **A 269** (1988) 483.
88Fai Faifman, M.P.: Muon Catalyzed Fusion **2** (1988) 247 and 285.
88Jae Jändel, M. et al.: Muon Catalyzed Fusion **3** (1988) 577.
88Hay Haywood, S.E. et al.: Phys. Rev. **A 37** (1988) 3393.
88Kam Kamimura, M.: Phys. Rev. **A 38** (1988) 621.
88Mar Markushin, V.E.: Muon Catalyzed Fusion **3** (1988) 395.
88Str1 Struensee, M.C., Cohen, J.S.: Phys. Rev. **A 38** (1988) 44.
88Str2 Struensee, M.C., et al: Phys. Rev. **A 37** (1988) 340.
88Vor Vorobyov, A.A., Petrov, Yu.V., Ponomarev, L.I. (eds.): Proceedings of μCF-87 (Gatchina); Muon Catalyzed Fusion **2/3** (1988).
89Ada Adamczak, A., Melezhik, V.S.: Muon Catalyzed Fusion **4** (1989) 303.
89Bre Breunlich, W.H., Kammel, P., Cohen, J.S., Leon, M.: Ann. Rev. Nucl. Sci. **39** (1989) 311.
89Bog Bogdanova, L.N. et al.: Sov. J. Nucl. Phys. **50** (1989) 848.
89Bra Bracci, L. et al.: Muon Catalyzed Fusion **4** (1989) 247.
89Coh Cohen, J.S.: Nucl. Instr. **B 42** (1989) 419.
89Har Hara, S., Ishihara, T.: Phys. Rev. **A 39** (1989) 5633.
89Jon Jones, S.E., Rafelski, J., Monkhorst, H.J. (eds.): Proceedings of μCF-88 (Sanibel Island); AIP Conference Proceedings **181** (1989).
89Kam1 Kamimura, M.: AIP Conference Proceedings **181** (1989) 330.
89Kam2 Kamimura, M.: private communication as reported in AIP Conference Proceedings **181** (1989) 27.
89Leo Leon, M.: Phys. Rev. **A 39** (1989) 5554.
89Men Menshikov, L.I. et al.: Sov. Phys. JETP **68** (1989) 258.
89Nag Nagamine, K.: Proc. Japan Academy **B 65** (1989) 225.
89Nae Nägele, N. et al.: Nuclear Physics **A 493** (1989) 397.
89Raf Rafelski, H.E. et al.: Prog. Part. Nucl. Phys. **22** (1989) 279.
90Bau Baumann, P. et al.: Muon Catalyzed Fusion **5/6** (1990/91) 87.
90Bog Bogdanova, L.N., Markushin, V.E: Muon Catalyzed Fusion **5/6** (1990/91) 189.
90Bre Breunlich, WH., Kammel, P., Marton, J., Zmeskal, J. (eds.): Proceedings of μCF-90 (Vienna); Muon Catalyzed Fusion **5/6** (1990/91).
90Dan Daniel, H.: Muon Catalyzed Fusion **5/6** (1990/91) 335.
90Hal Hale, G.M.: Muon Catalyzed Fusion **5/6** (1990/91) 227.
90Nag Nagamine, K., Matsuzaki, T., Ishida, K. et al.: Muon Catalyzed Fusion **5** (1990) 239.
90Pet Petitjean, C. et al.: Muon Catalyzed Fusion **5/6** (1990/91) 199.
90Pon Ponomarev. L.I.: Contemporary Phys. **31** (1990) 219.
90Sto Stodden, C.D. et al.: Phys. Rev. **A 41** (1990) 1281.
90Sza Szalewicz, K. et al.: Muon Catalyzed Fusion **5/6** (1990/1991) 241.
90Zme Zmeskal., J. et al.: Phys. Rev. **A 42** (1990) 1165.
91Cra Crawford, J.E. et al.: Phys. Rev. **D 43** (1991) 46.
91Fai Faifman, M.P., Ponomarev, L.I.: Phys. Lett. **B 265** (1991) 201.
91Fri Friar, J.L. et al.: Phys. Rev. Lett. **66** (1991) 1827.
91Kam Kamimura, M., private communication (1991).

91Jez Jeziorski, B. et al.: Phys. Lett. **A 43** (1991) 1640.
92Aba Abadjev, V.S. et al.: INR preprint **786/92** (1992).
92Dzh Dzhelepov, V.P. et al.: Sov. Phys. JETP **74** (1992) 589.
92Fro Frölich, P.: Advances in Physics **41** (1992) 405.
92Mar Markushin, V.E. et al.: Muon Catalyzed Fusion **7** (1992) 155.
92Pet Petitjean, C.: Nucl. Phys. **A 543** (1992) 79c-98c.
93Cas Case, T. et al.: Hyperfine Interactions **82** (1993) 295.
93Fro Frölich, P. (ed.): Proceedings of μCF-92 (Uppsala); Hyperfine Interactions **82** (1993).
93Ish Ishida, K. et al.: Hyperfine Interactions **82** (1993) 111.
93Ger Gershtein, S.S., Gusev, V.V.: Hyperfine Interactions **82** (1993) 185.
93Jon Jones, S.E., et al: Hyperfine Interactions **82** (1993) 303.
93Kin Kino, Y., Kamimura, M.: Hyperfine Interactions **82** (1993) 111.
93Kuz Kuzminov, V.V. et al.: Hyperfine Interactions **82** (1993) 423.
93Mar Markushin, V.E. et al.: Hyperfine Interactions **82** (1993) 373.
93Pet1 Petitjean, C.: PSI Report PSI-PR-93-09 (1993).
93Pet2 Petitjean, C. et al.: Hyperfine Interactions **82** (1993) 273.
93Scr Scrinzi, A. et al.: Phys. Rev. **A 47** (1993) 4691.
94Hu Hu, C.-Yu, Hale, G.M., Cohen, J.S.: Phys. Rev. **A 49** (1994) 4481.
94Kra Kravtsov, A.V. et al.: Z. Phys. **D 29** (1994) 49.
94Mor Morenzoni, E. et al.: Phys. Rev Lett **72** (1994) 2793.
95Fro Frölich, P. et al.: Phys. Rev. Lett. **75** (1995) 2108.
95Lat Latysheva, L.N. et al.: Hyperfine Interactions **101/102** (1996) 669.
95Nag Nagamine, K., Miyake, Y., Shimomura, K. et al.: Phy. Rev. Lett. **74** (1995) 4811.
95Sto Stolupin, V.A.: Nukleonika **40** (1995) 65.
96Ada Adamczak, A.: Hyperfine Interactions **101/102** (1996) 113.
96Coh Cohen, J., Hale, G.M., Hu, C.-Y.: Hyperfine Interaction **101/102** (1996) 349.
96Cza Czaplinski, W. et al.: Z. Phys. **D 37** (1996) 283.
96Dem Demin, D/L. et al.: Hyperfine Interactions **101/102** (1996) 13.
96Fai Faifman, M.P.: Hyperfine Interactions **101/102** (1996) 179.
96Gar Gartner, B. et al.: Hyperfine Interactions **101** (1996) 249.
96Kno Knowles, P.E. et al.: Hyperfine Interactions **101/102** (1996) 21.
96Kor Korobov, V.I.: Hyperfine Interactions **101/102** (1996) 329.
96Lau Lauss. B. et al.: Phys. Rev. Lett. **76** (1996) 4963.
96Mar1 Marshall, G.M. et al.: Hyperfine Interactions **101/102** (1996) 47.
96Mar2 Markushin, V.E.: Hyperfine Interactions **101/102** (1996) 155.
96Mel Melezhik, V.S.: Hyperfine Interactions **101/102** (1996) 365.
96Mol Molzon, W. et al.: UCI Physics Technical Report #96-30 (1996).
96Nag1 Nagamine, K., Matsuzaki, T., Ishida, K. et al.: Hyperfine Interactions **101/102** (1996) 521.
96Nag2 Nagamine, K.: Nucl. Phys. **A 51** (1996) 115.
96Pal Palmer, R. et al.: Nuclear Physics B (Proc. Suppl.) **A 51** (1996) 61.
96Pon Ponomarev, L.I., Petitjean, C., Bogdanova, K., Korobov, V.I., Markushin, V.E. (eds.): Proceedings of μCF-95 (Dubna); Hyperfine Interactions **101/102** (1996).
96Sak Sakamoto, S. et al.: Hyperfine Interactions, **101/102** (1996) 297.
96Str Strasser, P. et al.: Phys. Lett. **B 368** (1996) 32.
97Bad Baderscher, A. et al.: Phys. Lett. **B 392** (1997) 278.
98Ish Ishida, K., Nagamine, K.: KEK Proceedings **98-5 II** (1998) 12.
98Nag Nagamine, K., Kamimura, M.: Adv. Nucl. Phys. **24** (1998) 151.
99Ack Ackerbauer, P. et al.: Nucl. Phys. **A 652** (1999) 311.
99Bog Bogdanova, L.N., Korobov, V.I., Ponomarev, L.I.: Hyperfine Interactions **118** (1999) 183.
99Kaw Kawamura, N. et al.: Phys. Lett. **B 465** (1999) 74.
99Liu Liu, W. et al.: Phys. Rev. Lett. **82** (1999) 711.

99Mat Matsuzaki, T. et al.: Hyperfine Interactions **119** (1999) 361.
99Mul Mulhauser, M. et al.: Hyperfine Interactions **119** (1999) 305.
99Pet1 Petitjean, C., Schaller, L.A., Markushin, V., Mulhauser, F., Simmons, L. (eds.): Proceedings of EXAT-98 (Ascona); Hyperfine Interactions **119** (1999).
99Pet2 Petitjean, C.: Hyperfine Interactions **118** (1999) 127.
99Yuk Yukhimchuk, A. et al.: Hyperfine Interactions **119** (1999) 341.
00Fai Faifman, M: private communication (2000).
00Fuj Fujiwara, M.C. et al.: Phys. Rev. Lett. **85** (2000) 1642.
00Ish Ishida, K.: private communication (2000).
00Nak Nakamura S.N. et al.: Phys. Lett. **B 473** (2000) 226.
01Ada Adamczak, A. and Faifman, M.P.: Phys. Rev. **A 64** (2001) 052705
01Ani Anissimov, V.V. et al., Fusion Technology **39** (2001) 198.
01Bak Bakalov, D., Korobov, V.I.: Hyperfine Interactions **138** (2001) 265.
01Bom Bom, V.R. et al.: Hyperfine Interactions **138** (2001) 213.
01Bro Brown, H.N. et al.: Phys. Rev. Lett. **86** (2001) 2227.
01Mat Matsuzaki, T. et al.: Nucl. Instruments **A 465** (2001) 365.
01Pet Petitjean, C.: Hyperfine Interactions **138** (2001) 191.
01Por Porcelli, T.A. et al.: Phys. Rev. Lett. **86** (2001) 3763.
01Toy Toyoda, A. et al.: Phys. Lett. **B 509** (2002) 30.
01Vor Voropaev, N.I. et al.: Hyperfine Interactions **138** (2001) 331.
02Ish Ishida, K, Nagamine, K. (eds.) : Proceedings of μCF-01 (Shimoda); Hyperfine Interactions (2002) in press.
02Mat Matsuzaki, T. et al., Nucl. Instruments **A 408** (2002) 814.
03Ish Ishida, K., Nagamine, K., Matsuzaki, T. et al.: Phys. Rev. (2003) to be published.
03Kaw Kawamura, N. et al.: Phys. Rev. Lett. **90** (2003) 043401.
03Toy Toyoda, A. et al.: Phys. Rev. Lett. **90** (2003) 243401.